frontiers | Frontiers in Earth Science

TYPE Original Research
PUBLISHED 31 March 2025
DOI 10.3389/feart.2025.1563011

OPEN ACCESS

EDITED BY
Alexis Godet,
University of Texas at San Antonio,
United States

REVIEWED BY
Adriano Guido,
University of Calabria, Italy
Xiaobing Wu,
Wuhan University, China

*CORRESPONDENCE
Min Zhang,
mzhang@hgnu.edu.cn

RECEIVED 18 January 2025
ACCEPTED 05 March 2025
PUBLISHED 31 March 2025

CITATION
Li H and Zhang M (2025) Spatio-temporal distribution of global stromatolites through geological time identified by a large language model approach.
Front. Earth Sci. 13:1563011.
doi: 10.3389/feart.2025.1563011

Spatio-temporal distribution of global stromatolites through geological time identified by a large language model approach

Hao Li[1] and Min Zhang[2]*

[1]School of Earth Resources, China University of Geosciences, WuHan, Hubei, China, [2]School of Geography and Tourism, Huanggang Normal University, Huanggang, Hubei, China

Introduction: A substantial amount of data embedded within diverse literature makes it time-consuming to manually extract and compile extensive datasets. The use of large language models has become essential for the efficient extraction and analysis of big data. This study utilizes ChatGPT-4 to reconstruct a global database of stromatolites, spanning from the Precambrian to the present, to enhance our understanding of their spatial and temporal dynamics throughout geological time.

Methods: The data extraction process involved several steps: First, PDF documents containing stromatolite literature were gathered and converted into text format. Second, ChatGPT-4 was employed to extract data on stromatolite occurrences, including locations, ages, strata, and facies types from each sentence in the documents. Third, duplicates were removed, and the data were organized into three categories: 3,248 unique location-age pairs, 2,723 strata-age pairs, and 1,723 strata-age-facies type combinations. Additionally, 2,565 paleogeographical locations of stromatolite-bearing rocks were reconstructed using modern latitude and longitude coordinates and corresponding Phanerozoic ages.

Results: The newly obtained dataset reveals that stromatolite occurrences peaked during the Proterozoic, declined during the Early Phanerozoic, and exhibited fluctuations throughout the Phanerozoic. Seven global stromatolite hotspots were identified: the United States, Australia, India, Canada, China, England, and Russia. From the Cambrian to the Jurassic, stromatolites were predominantly distributed in low and middle latitudes, shifting to higher latitudes from the Cretaceous to the Quaternary. The proportion of inland aquatic stromatolites relative to marine stromatolites varied, ranging from 10% to 30% from the Mesoarchean to the Middle Mesoproterozoic, decreasing to less than 10% from the Late Mesoproterozoic to the Early Paleozoic, increasing to 10%–30% from the Devonian to the Jurassic, and remaining high (39%–53%) from the Cretaceous to the Quaternary.

Discussion: The findings highlight the temporal and spatial variability of stromatolite occurrences, shedding light on the evolution of these microbial structures over geological time. The distribution patterns suggest significant shifts in environmental conditions and provide valuable insights into paleogeographical and ecological dynamics. The use of ChatGPT-4 to extract

and organize data from a large body of literature demonstrates the potential of large language models for advancing research in paleobiology and geology.

KEYWORDS

large language model, stromatolites, spatio-temporal distribution, sedimentology, deep time

1 Introduction

In Earth science, vast amounts of information are archived in diverse types of literature, including peer-reviewed journals, databases, research reports, survey reports, and books. Constructing reviews or meta-analyses in geosciences often requires extensive data compilation, which is frequently fragmented and time-consuming when done manually. Recently, large language models, such as ChatGPT, have demonstrated exceptional performance in various natural language processing tasks, including question answering, machine translation, and text generation. ChatGPT's capabilities have been effectively applied in fields such as medicine (Fuchs et al., 2024), healthcare (Li et al., 2024), and physics education (Polverini and Gregorcic, 2024). Furthermore, the principles of large language models have been utilized for geological applications, including soil science research (Cahyana et al., 2024), seismic engineering (Ray, 2024), and remote sensing (Osco et al., 2023).

In this study, we employ the large language model ChatGPT-4 to develop a comprehensive database of global stromatolite occurrences throughout geological time. Notably, this approach allows for the extraction of sample features without the need for exhaustive manual search, significantly reducing the labor required for our study. Modern stromatolites are actively investigated across various fields, including biology, Earth science, environmental science, and climate change research. Key areas of focus include microbial composition and ecological roles, biogeochemical processes, environmental change recordings and impacts, and conservation and management efforts (Toneatti et al., 2017; Hohl and Viehmann, 2021; Carvalho et al., 2018; Vasconcelos et al., 2020). The study of ancient stromatolites is crucial for understanding Earth's early environments and the evolution of life. It provides valuable insights into geological records, environmental reconstruction, biological evolution, early Earth climate models, ancient ecosystem functions, microbial geochemical processes, applied technology development, and interdisciplinary research (Hohl and Viehmann, 2021; Martin-Bello et al., 2019; Petrash et al., 2016; Lan et al., 2020; Babilonia et al., 2018).

Most previous studies on stromatolite abundance have concentrated on specific time intervals, with few considering temporal changes in stromatolite populations. Peters et al. (2017) utilized the GeoDeepDive method to gather stromatolite occurrence data from the Precambrian to the present in North America (Peters et al., 2017). Zhang et al., (2023) developed a novel machine learning approach to extract global stromatolite occurrence data. The advancement of new methods and the accumulation of additional data will enhance our understanding of the spatio-temporal distribution patterns of stromatolites (Zhang et al., 2023).

This study aims to use stromatolites as a case study and apply a large language model approach to extract extensive occurrence data of stromatolites from the Precambrian to the present, including details on location, age, strata, and facies. The goal is to evaluate their global distribution patterns both temporally and spatially.

2 Data and method

The specific workflow of this study is divided into six steps, as shown in Figure 1. Each part is explained in detail as follows:

In Step A, we use the software DocumentCollector to perform full-text searches on websites like Elsevier, Wiley, Geoscienceworld, etc., using keywords to obtain the corresponding document titles and DOI numbers. Then, we use the software PaperDownloader to download the available online documents. At the same time, we can add locally accumulated relevant files to increase the data size, which forms our dataset for extraction. These two software tools can be obtained from https://github.com/Knowledge-Engineering-with-Big-Data.

After obtaining the relevant literature PDFs, in Step B, we used Tesseract OCR to process them into text documents and stored them in an Excel file. Tesseract is an optical character recognition tool developed by Google, which supports recognition of languages such as English from images and converts them into text format. It has stable and high-precision performance, so we chose this tool directly. This is a very routine process, and we will keep the converted TXT files. As the number of tasks increases, our dataset will grow, providing more data sources for future research.

In Step C, we use concurrent Spacy to segment the text obtained in Step B into sentences and extract sentences that contain target entities (for example, sentences that include keywords like "stromatolite," "strata," "location," or "geological age") as sentences to be extracted. Spacy is a highly accurate, scalable Natural Language Processing (NLP) tool suitable for industrial use, and it is built with Python code, which facilitates our calls and allows us to perform both rule-based and automatic initial extraction of candidate sentences. We use rule-based methods and dictionaries to obtain sentences containing relevant entities. These sentences are the ones to be extracted, such as those based on commonly used geological age phrase dictionaries, mineral dictionaries, paleontology dictionaries, and environmental description dictionaries. This step is mainly designed for efficiency and accuracy, enabling the later extraction process based on large language models to be more efficient and precise.

For example, in this step, we obtained a sentence: "Stromatolites from the Aptian Crato Formation, a hypersaline lake system in the Araripe basin, northeastern Brazil," which contains "Stromatolites," the location "Araripe basin," and the time age "Aptian."

In Step D, the prompts are adjusted and optimized on the web of ChatGPT for different extraction tasks to obtain the best-performing prompts. The detailed process is shown in Table 1.

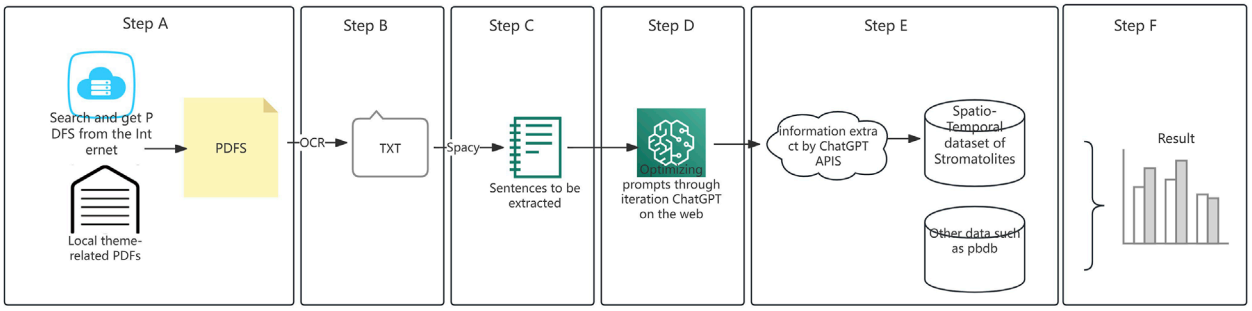

FIGURE 1
The workflow of this paper.

TABLE 1 Prompt optimization algorithm.

Input: Prompt + Dataset to be extracted + Detailed supplementary instructions **Output**: Data in a composite analysis format, such as JSON or Excel 1: Write the extraction prompts based on subject knowledge and extraction requirements. 2: Randomly select several datasets for extraction. 3: while (the extraction results from step 2 do not meet the requirements) 4: Optimize the prompt and repeat steps 1 and 2. 5: end 6: Perform extraction on the full text. 7: end

TABLE 2 The pseudocode for invoking ChatGPT-4 to process literature.

Response = ChatGPT-4_API (Prompts + text) Json = json.load (Response) Save (text, json)

An example for extracting the location, geological age, and stratum of stromatolites is as follows:

Prompt = Assume you are an excellent geologist. Extract the geological age, location, and stratum of the stromatolites from the content within the <text > tag. Return the result in JSON format with the following structure: {location: "", geological time: "", stratum: ""}. If the information cannot be determined from the literature, return "uncertain". <text>xxxx</text>

In step E, for the sentences obtained in Step C, we will use the prompts obtained in Step D combined with the ChatGPT-4 API for extraction and reading. The process for extracting text using LLM for information extraction and understanding is as follows in Table 2.

The above process is roughly divided into two parts. First, by calling the ChatGpt-4 API we extract and read the relevant information from the sentence and return it in a formatted way. For example, for the sentence above, we would obtain something like {location: "Araripe basin", geotime: "Aptian"}.

Then, the returned content is stored locally for final analysis.

Step F: The obtained data is analyzed, organized, and compared with data from other databases, such as PBDB (https://paleobiodb.org) and Geowhen (https://timescalefoundation.org/).

Here is the entire detailed workflow. The relevant code above can be found at https://github.com/severus-lee/code_Spatio-Temporal-Distribution-of-Global-Stromatolites-Through-Geological-Time.

2.1 Location mention extraction

Most location mentions extracted using ChatGPT-4 were specific localities (including countries, provinces, cities, counties, sections, regions, ranges, mountains, etc.), with a few referring to sedimentary facies (such as basins or marine environments), strata, or author addresses. Location mentions that referred to specific localities were retained, while others were discarded. The ArcGIS geocoding service was used to obtain the latitude coordinates for these geographical mentions. Mentions that could not be geocoded were removed. During the deduplication process of location-age pairs, locations with inclusion relationships were assessed, and the most accurate mention within the same age unit was retained. For instance, if the mentions included Guangxi Province-Induan, Tiandong County, Guangxi-Induan, and Zuodeng Section, Tiandong County, Guangxi Province-Induan, we retained only the last pair mention which is the most specific location and removed the others. This approach ensures that different location mentions within the same age unit represent distinct stromatolites and minimizes duplication. When multiple localities with identical longitude and latitude in the same age unit were extracted, only one pair mention was retained.

2.2 Age mention extraction

Most age mentions extracted using ChatGPT-4 include geological time units (Eon, Era, Period, Epoch, Age, Subage) and absolute ages. Absolute ages were converted to geological time units: Age for the Phanerozoic and Period for the Precambrian. Subages were merged into Ages based on the international chronostratigraphic chart. If a stromatolite occurrence spanned two adjacent ages within the Phanerozoic or two adjacent periods in the Precambrian, the occurrence was counted for both ages or periods. Gplates by Müller et al. (2022) was used to reconstruct stromatolite distributions through geological time and to obtain

paleolatitude coordinates based on absolute age and modern longitude and latitude.

2.3 Strata mention extraction

After extracting Strata-Age pairs using ChatGPT-4, duplicates in stratigraphic units were removed by omitting terminal words such as "Formation", "Group" "Limestone" and "Sandstone" to eliminate repetitive expressions of the same units. This process resulted in the identification of 421, 495, 457, and 385 unique Strata-Age pair data items, which were accurately classified to Age and Epoch time units within the Phanerozoic eon, and to Period and Era time units within the Precambrian eon. These data items are valid and available after the removal of duplicates.

2.4 Facies mention extraction

After extracting Facies-Strata pairs using ChatGPT-4, duplicate stratigraphic units were removed in a manner similar to the Strata mentions. The age of each stratum was used as the age for the Facies-Strata pairs. The extracted facies mentions were categorized into facies types of stromatolite-bearing strata, including shelf, shoal, tidal, lagoon, delta, glacial, and inland aquatic facies. The Archean and Proterozoic of the Precambrian, along with 12 periods of the Phanerozoic (from the Cambrian to the Quaternary) and Recent, were selected as time bins. An occurrence dataset of stromatolites was obtained by extracting Facies-Strata pairs. Proportional occurrences of global stromatolites in these seven environmental types were calculated based on the extracted results of stromatolite strata versus shelf, shoal, tidal, lagoon, delta, glacial, and inland aquatic facies across these 15 time intervals.

3 Results

3.1 Data items

A total of 11,678 documents are collected which contained the terms "stromatolite(s)" or "stromatolitic". We employed large language model techniques to extract information on stromatolites concerning their location, age, strata, and facies from these scientific papers. From the dataset, we obtained a total of 40,549 sentences related to stromatolites. After removing duplicates, there were 3,248, 2,723, and 1,723 unique and valid pair mentions of stromatolites versus locations and ages, strata and ages, and strata, ages, and facies, respectively. In total, 5,971 unique data items were valid and available after merging the four types of mentions from the datasets.

In this study, we utilize a comprehensive global stratigraphic database to normalize and measure the frequency of stromatolite occurrences, considering variations in the total stratigraphic quantity of sedimentary rocks. Our dataset comprises 17,274 collections from the Paleobiology Database (PBDB, https://paleobiodb.org), encompassing 32,866 stratigraphic units. Additionally, it includes the database of Cantine et al. (2020), which covers 259 stratigraphic units of Precambrian carbonates, along with the stromatolite-bearing stratigraphic units identified in this study. Together, these form the total stratigraphic database of rocks used for our analysis.

The animal genus-level diversity of Phanerozoic carbonates was estimated using 7,332 collections from the Paleobiology Database (PBDB, https://paleobiodb.org) that are associated with carbonate stratigraphic units. The taxonomy for each stratigraphic unit is accessible through the PBDB's programmatic interface (Peters and McClennen, 2016). To account for variation in rock quantity, genus-level diversity in each epoch or age was normalized by dividing it by the total number of carbonate units.

3.2 Temporal distribution patterns of global stromatolites from precambrian to recent

The extraction of Stromatolite-Age-Locality mentions was performed using a large language model approach to analyze the secular changes in stromatolite distribution worldwide from the Precambrian to the present. The age mentions were categorized into five levels: Eon, Era, Period, Epoch, and Age. The global dataset reveals that stromatolite occurrence abundance follows three distinct stages: relatively low in the Archean, a high plateau during the Proterozoic, and a relatively low level during the Phanerozoic at the eon level. At the era level, stromatolites were relatively rare in the Eoarchean and Neoarchean, rebounded during the Paleoarchean and Neoarchean, and then experienced stepwise increases from the Paleoproterozoic to the Neoproterozoic, peaking in the Neoproterozoic during the Precambrian. This was followed by significant declines during the Paleozoic and Mesozoic and a subsequent rebound in the Cenozoic during the Phanerozoic (Figures 2A, B).

At the period level, global stromatolite records were sparse during the Paleoproterozoic and Mesoproterozoic, except for high values observed in the Orosirian and Calymmian periods. A rapid increase occurred from the Mesoproterozoic to the Neoproterozoic, with the highest levels in the Ediacaran of the Late Neoproterozoic during the Precambrian, followed by pronounced increases in the Cambrian and Ordovician periods (Figures 2A, B). During the Phanerozoic, stromatolite occurrence abundance fluctuated at the period level, showing pronounced peaks in the Cambrian, Triassic, and Quaternary, with relatively higher values during the Neogene (Figure 2B).

At the epoch level, the global record of stromatolites showed slight fluctuations from the Cambrian to the Early Ordovician, followed by a rapid decrease in the Middle Ordovician and a gradual increase from the Late Ordovician to the Late Silurian. The occurrence slightly fluctuated during the Devonian and Early Carboniferous, then declined in the Late Carboniferous and remained at a low level until the Guadalupian. This was followed by an abrupt increase in the Lopingian and Early Triassic, and then a rapid decline in the Middle Triassic. From the Middle Triassic to the present, fluctuations were moderate, with pronounced peaks in the Miocene of the Neogene, and the Pleistocene and Holocene of the Quaternary (Figure 2B). The stratigraphic resolution of Precambrian stromatolite records is too low to indicate reliable secular change trends during the Precambrian at the epoch and age levels.

At the age level, the global record of stromatolites exhibited high values in the Fortunian of the Early Cambrian, low values in

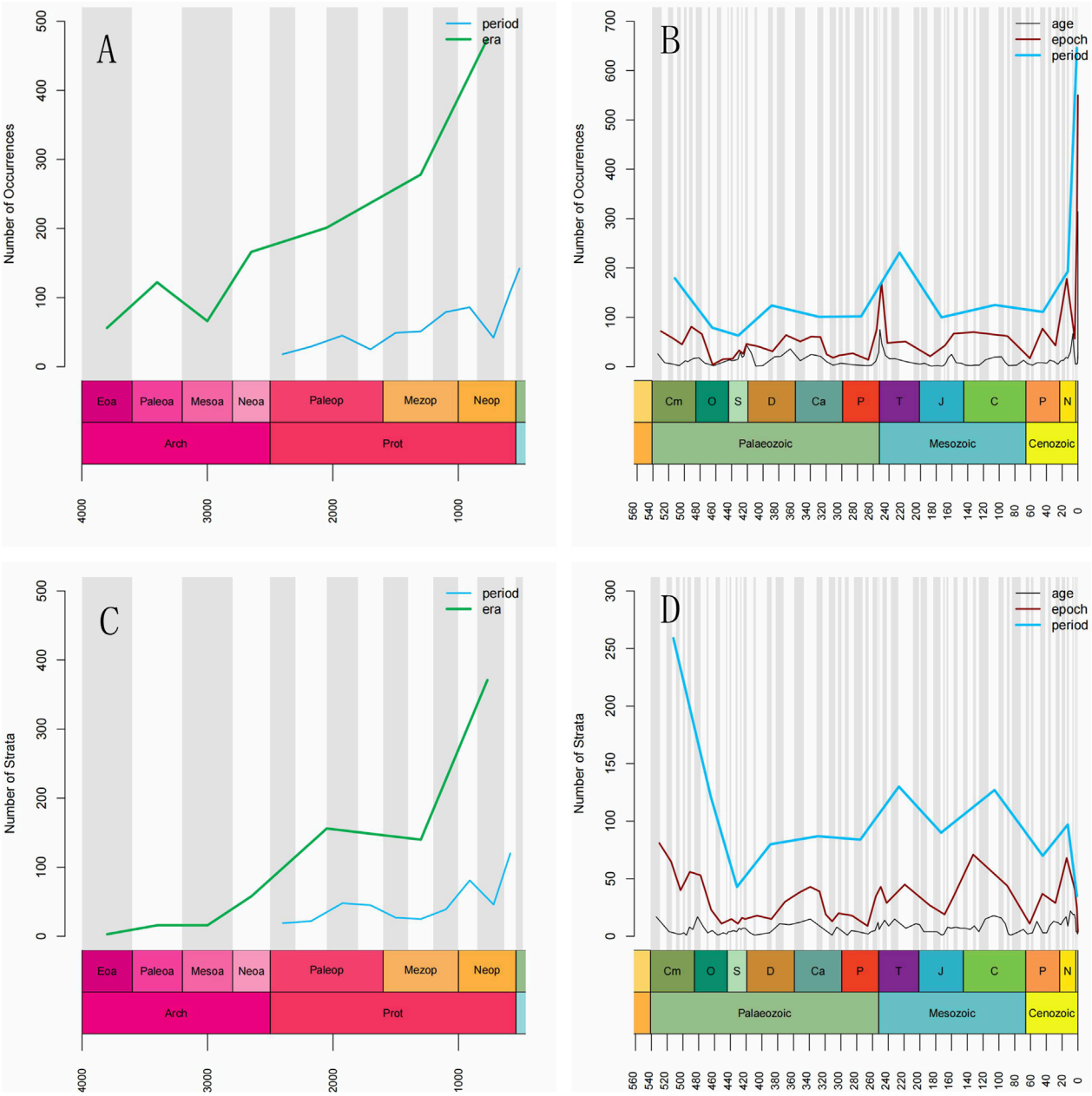

FIGURE 2
(A) Distribution patterns of the occurrence abundance of global stromatolites at the Era and Period levels in Precambrian, based on the extraction of paired mentions of "stromatolite-locality-age". **(B)** Distribution patterns of the occurrence abundance of global stromatolites at the Period, Epoch, and Age levels in Phanerozoic, based on the extraction of paired mentions of "stromatolite-locality-age". **(C)** Distribution patterns of the occurrence abundance of global stromatolites at the Era and Period levels in Precambrian, based on the extraction of paired mentions of "stromatolite-strata-age". **(D)** Distribution patterns of the occurrence abundance of global stromatolites at the Period, Epoch, and Age levels in Phanerozoic, based on the extraction of paired mentions of "stromatolite-strata-age". Abbreviations: Eoa, Eoarchean; Paleoar, Paleoarchean; Mesoar, Mesoarchean; Neoar, Neoarchean; Paleop, Paleoproterozoic; Mezop. Neop, Neoproterozoic; Cm, Cambrian; O, Ordovician; S, Silurian; D, Devonian; Ca, Carboniferous; P, Permian; T, Triassic; J, Jurassic; C, Cretaceous; Pg, Paleogene; N, Neogene; Q, Quaternary.

Series 2 and the Drumian of the Miaolingian, and moderate values from the Guzhangian of the Miaolingian in the Cambrian to the Tremadocian of the Early Ordovician. The values then declined to a low point from the Floian of the Early Ordovician to the end of the Ordovician. Stromatolite occurrences surged and reached a plateau from the Homerian of the Wenlock in the Silurian to the Lochkovian at the beginning of the Devonian, and again from the Givetian of the Middle Devonian to the Serpukhovian of the Mississippian in the Early Carboniferous, with low values in the Pragian and Emsian of the Early Devonian. The record declined to a low value in the Bashkirian of the Early Pennsylvanian and remained low until the Capitanian of the Guadalupian in the Middle Permian.

This was followed by a rapid increase from the Wuchiapingian of the Lopingian in the Late Permian to the Induan of the Early Triassic, with a stepwise decrease from the Olenekian in the Early Triassic to the Aalenian of the Middle Jurassic. Slight fluctuations occurred from the Middle Jurassic to the present, with high values in the Oxfordian of the Upper Jurassic, the Tortonian of the Upper Miocene to the Zanclean of the Early Pliocene in the Neogene, and the Upper Pleistocene to the Greenlandian of the Holocene in the Quaternary (Figure 2B). There were pronounced peaks in the Messinian of the Neogene and the Meghalayan in the Late Quaternary.

3.3 Stratigraphical distribution patterns of global stromatolites in geological time

The patterns of global stromatolite distributions over geological time may be influenced by sampling bias. Stromatolite occurrence abundance from stratigraphic units that were more intensely studied during particular time intervals may appear much higher than in those that were less studied. To minimize sampling bias, we counted the number of stromatolite-bearing stratigraphic units from each time interval and compared these counts with the occurrence abundance of stromatolites from the same intervals.

The number of stromatolite-bearing stratigraphic units from each time interval was determined by extracting mentions of "stromatolite-strata-age" relationships. In total, 2,723 stratigraphic units were identified from time intervals, accurately categorized to the epoch or age levels in the Phanerozoic and to the period or era levels in the Precambrian, that yield stromatolites.

The results show that the global records of stromatolite-bearing stratigraphic units are low in the Archean, relatively high in the Proterozoic, and high during the Phanerozoic at the eon level. The occurrence abundance of stromatolite-bearing units remained low in the Archean, gradually increased throughout the Proterozoic and Paleozoic, and then declined in the Mesozoic and Cenozoic at the era level (Figures 2C,D).

At the period level, the global record of stromatolite-bearing units shows low values with slight fluctuations during the Paleoproterozoic and Mesoproterozoic (Figure 2C). This is followed by a stepwise increase from the Neoproterozoic to the Cambrian, a pronounced decline during the Ordovician and Silurian, and fluctuating values from the Devonian to the Quaternary, with notable peaks in the Triassic and Cretaceous (Figure 2D).

At the epoch level, the number of stromatolite-bearing units plateaued during the Cambrian to Early Ordovician, was relatively high during the Upper Devonian to Upper Mississippian in the Carboniferous, the Lopingian in the Permian-Triassic, the Upper Jurassic-Cretaceous, the Eocene in the Paleogene, and the Pleistocene in the Quaternary. Significant peaks were observed during the Terreneuvian-Series 2, Early Ordovician, Early Cretaceous, and Miocene epochs, respectively (Figure 2D).

At the age level, peaks in the global records of stromatolite-bearing units occurred in the Fortunian of the Early Cambrian, Tremadocian of the Early Ordovician, Visean of the Early Carboniferous, Carnian of the Late Triassic, Aptian, Albian, and Cenomanian of the Early to Middle Cretaceous, Langhian of the Middle Miocene, and from the Tortonian to the Piacenzian of the Late Miocene to Pliocene (Figure 2D).

3.4 Relative abundance of global stromatolites compared to sedimentary rocks and carbonates

The question of whether some Archean stromatolite structures formed due to biological activity remains open (Lowe, 1994). At the period level, stromatolites are present in approximately 55% of all named sedimentary units in the Early Paleoproterozoic, increasing to 75% in the Late Paleoproterozoic (Figure 3). During the Middle Mesoproterozoic, stromatolite occurrences decline to 47%, but they rise again to about 60% by the end of the Mesoproterozoic. After peaking in the Tonian, stromatolite occurrences decrease to 70%–80% in the Middle to Late Neoproterozoic. Stromatolite occurrences rapidly decline to 30% in the Cambrian and remain at no more than 10% for the remainder of the Phanerozoic. Normalizing stromatolite prevalence by the number of named carbonate-bearing sedimentary units (Figure 3) shows broadly similar patterns. However, during some periods in the Proterozoic, over 80% of all named carbonate-bearing lithostratigraphic rock units contain stromatolites.

At the epoch level in the Phanerozoic, stromatolites occur in over 10% of all named sedimentary units during the Cambrian to Early Ordovician, Early Mississippian, Late Mississippian, and Early Triassic. Stromatolites are present in over 20% of all named carbonate-bearing lithostratigraphic rock units during the Terreneuvian and Furongian of the Cambrian in the Paleozoic, Early Triassic in the Mesozoic, Pliocene of the Paleogene, and Holocene of the Quaternary in the Cenozoic.

3.5 Correlation between the abundance of stromatolites, biodiversity, and dolomites in carbonates

We use the Spearman correlation coefficient ρ, a non-parametric statistical method to assess monotonic relationships between variables. The Spearman correlation coefficient ranges from −1 to +1: +1 indicates a perfect positive correlation, −1 indicates a perfect negative correlation, and 0 indicates no correlation. The statistical significance of the correlation is determined by the p-value, which indicates whether the observed correlation is statistically significant. A p-value of 0.05 or less is generally considered significant.

At the age level, there is a negative correlation ($\rho = -0.47$, $P = 0.042$) between average metazoan genus-level diversity and stromatolite prevalence in carbonate-bearing rock units from the Guzhangian of the Middle Cambrian to the Pridoli of the Latest Silurian (Figure 4A). A similar negative correlation ($\rho = -0.254$, $P = 0.048$) exists from the Frasnian of the Upper Devonian to the Serravallian of the Middle Neogene (Figure 4A). The correlation between animal genus-level diversity and stromatolite abundance in the Phanerozoic was not statistically significant over 10 ages in other periods.

At the age level, there is a positive correlation ($\rho = 0.314$, $P = 0.035$) between dolomitic carbonate units and stromatolite prevalence in carbonate-bearing rock units from the Fortunian of the Early

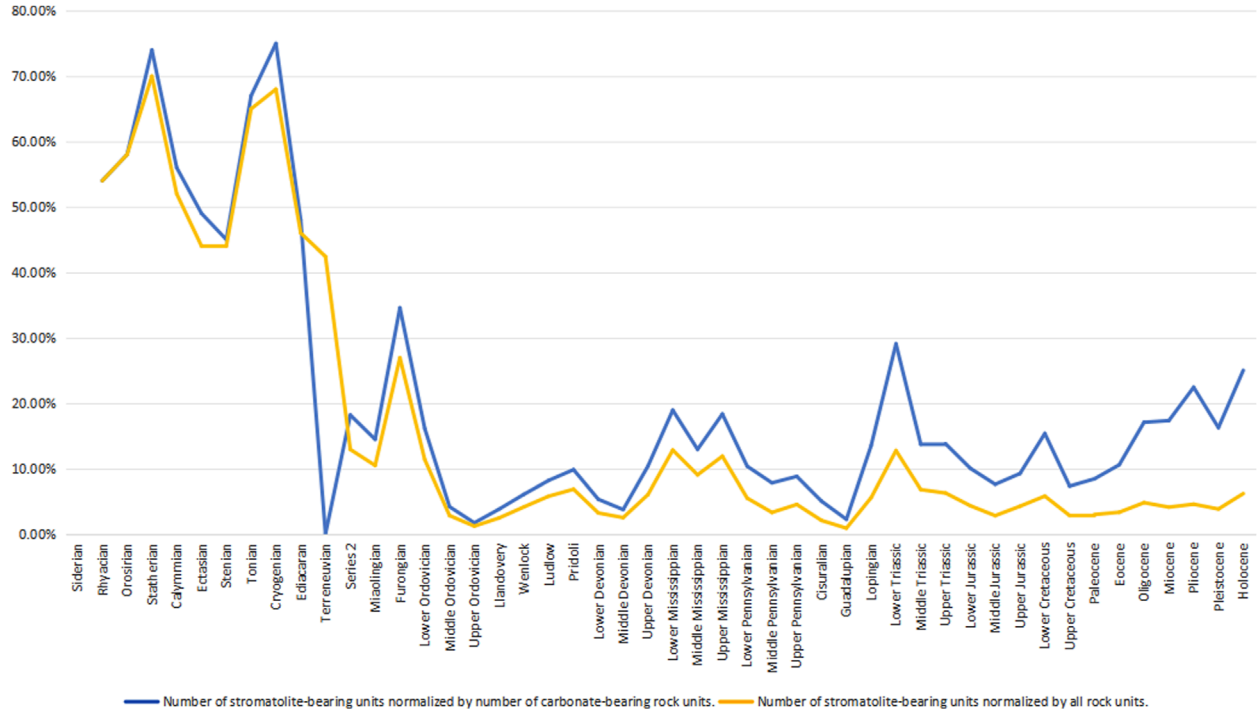

FIGURE 3
Occurrence of stromatolites over geological time normalized by total number of sedimentary rock units.

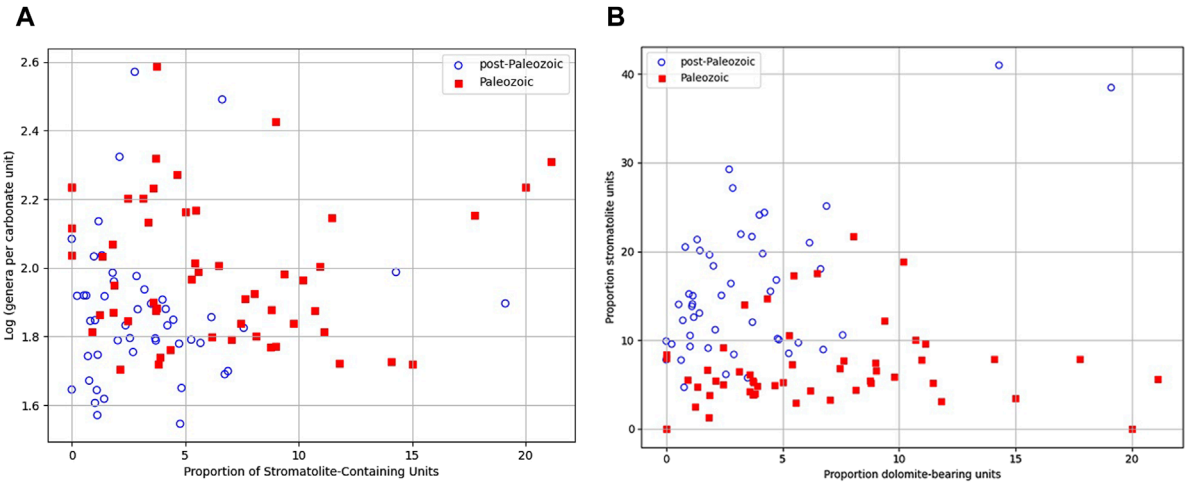

FIGURE 4
Proportion of dolomite-bearing carbonate units and genus diversity in relation to stromatolite prevalence. **(A)** Logarithm of average genus diversity versus stromatolite prevalence in carbonates. See text for correlation coefficients. **(B)** Stromatolite prevalence (from Figure 3B) versus the proportion of dolomitic carbonates in carbonates during the Phanerozoic.

Cambrian to the Wuchiapingian of the Late Permian when the data are detrended by taking first differences (Figure 4B). A similar positive correlation ($\rho = 0.454$, $P = 0.044$) exists from the Hettangian of the Early Jurassic to the Maastrichtian of the Late Cretaceous (Figure 4B). The correlation between dolomitic carbonate units and stromatolite prevalence in carbonate-bearing rock units was not statistically significant across 10 other ages in the Phanerozoic.

3.6 Locality distributions of global stromatolites

To illustrate the geographical distribution pattern of global stromatolites based on the extracted information, the coordinates of the extracted locations were obtained. We used the paleogeographical reconstruction method based on Müller et al.

(2022) to estimate the paleogeographical locations of stromatolite-bearing rocks at the epoch level of the Phanerozoic. A total of 2,565 paleogeographical locations of stromatolite-bearing rocks were recovered using modern latitude and longitude data and corresponding ages in the Phanerozoic. These data points were plotted onto paleogeographical maps according to the ages of the stromatolites using paleolongitudes and paleolatitudes of the localities based on the model by Müller et al. (2022).

In the Early Paleozoic, stromatolites were most prevalent in North America, with the exception of the Terreneuvian of the early Cambrian, where they were more common in Asia. Stromatolites were present in Africa at a rate of 3%–13%, except during the Middle Ordovician when they rose to 25%. In Oceania, stromatolites comprised less than 12% of occurrences, while in Antarctica, they accounted for less than 2%. South America had less than 5% of stromatolite occurrences. In Europe, stromatolites accounted for 8%–25% of occurrences from the Cambrian to the Llandovery of the early Silurian, increasing to 30%–42% from the Wenlock to the Pridoli of the Silurian. In North America, stromatolites constituted 20%–25% of occurrences during the Terreneuvian and Series 2 of the early Cambrian, rising to 42%–70% during other epochs of the Early Paleozoic. In Asia, stromatolites were present in 10%–33% of occurrences from the Cambrian to the Wenlock of the Silurian, with a notable decline to 3%–4% during the Ludlow and Pridoli of the Late Silurian.

In the Late Paleozoic, stromatolites were most prevalent in Europe, accounting for 19%–47% of occurrences, and in North America, where they constituted 20%–58% of occurrences. In Asia, stromatolites were less common, making up less than 25% of occurrences. In Africa, stromatolites were found in 5%–7% of occurrences during the Devonian, 11%–20% during the Carboniferous, and 3% during the Late Permian. Oceania had less than 8% of stromatolite occurrences, except for a peak of 19% in the Late Devonian. South America had less than 6% of occurrences, and Antarctica had less than 2%. The proportion of stromatolites was highest in Europe during the Middle Devonian, the Middle Mississippian of the Carboniferous, and the Cisuralian and Lopingian of the Permian. In North America, stromatolites were more prevalent during other epochs of the Late Paleozoic.

In the Mesozoic, stromatolites were most prevalent in Europe, accounting for 21%–59% of occurrences, and in North America, where they constituted 18%–37%. In Asia, stromatolites occurred in 30%–40% of instances during the Early to Middle Triassic and in 7%–20% during the Late Triassic. In Africa, stromatolites accounted for 3%–21% of occurrences, while in Oceania and South America, they made up less than 10%. Stromatolites were most prevalent in North America during the Early Triassic and Early Jurassic, while in Europe, they dominated during other epochs of the Mesozoic.

In the Cenozoic era, stromatolites were most prevalent in North America, where they accounted for 19%–54% of occurrences. In Europe, stromatolites made up 27%–55% of occurrences during the Paleogene and Neogene, and 14%–19% during the Quaternary. In Africa, stromatolites accounted for 9%–15% of occurrences, while in Asia, they constituted 6%–18%. Oceania had less than 10% of stromatolite occurrences, and South America had less than 5%, except for a peak of 29% in the Paleocene. Antarctica had less than 1% of occurrences. Stromatolites were most prevalent in Europe during the Paleocene, Oligocene, and Miocene, while North America dominated in other epochs of the Cenozoic.

In recent times, stromatolites are found in 40% of occurrences in North America, 23% in Europe, 8% in Africa, 13% in Asia, 9% in Oceania, 5% in South America, and less than 1% in Antarctica.

A heat map of the extracted sites reveals seven major hotspots for global stromatolite records: the USA, Australia, India, Canada, China, England, and Russia. These sites cover a broad range of regions worldwide (Figure 5), suggesting that sampling bias in the data sources for global stromatolites is relatively minimal. The top ten countries with the highest frequency of occurrence is illustrated in Table 3.

3.7 Latitudinal distribution of stromatolites in the phanerozoic

Data for this analysis were gathered by extracting Locality-Age pairs of stromatolites using ChatGPT-4 and removing duplicates. We then utilized the paleogeographical reconstructions from Müller et al. (2022) to estimate the Phanerozoic paleolatitudes of stromatolite-bearing localities. The results are shown in Figure 6.

At the epoch level, when the paleolatitudinal data are divided into 30° bins, the proportion of stromatolites in the 0°–30° bin ranged from 50% to 60% during the Terreneuvian to Series 2 of the Cambrian, and from 30% to 50% in the Miaolingian to Furongian of the Cambrian. This proportion rebounded to 50%–60% in the Lower to Middle Ordovician and remained high (60%–90%) until the Lower Cretaceous, then decreased to 14%–47% after the Lower Cretaceous. The proportion in the 30°–60° bin was 40%–67% during the Cambrian to Middle Ordovician, except for 36% in the Lower Ordovician. It fell below 40% from the Late Ordovician to the Lower Cretaceous but increased to 60%–70% from the Upper Cretaceous to the Holocene, with notable values of 47% in the Paleocene and 83% in the Oligocene. The proportion in the 60°–90° bin was below 6% except for 9% in the Upper Ordovician. The median paleolatitudes of all localities were 26°–35° in each epoch of the Cambrian, 8°–25° from the Ordovician to the Jurassic, and 27°–41° from the Cretaceous to the Quaternary.

The lower proportion of stromatolites at low paleolatitudes (0°–30°), the relatively higher proportion at middle paleolatitudes (30°–60°), and the higher median paleolatitudes of all localities in the Cretaceous to Quaternary compared to those in the Ordovician to Jurassic suggest a migration of stromatolites toward higher paleolatitudes during the Cretaceous to Quaternary.

3.8 Temporal variation of sedimentary facies of global stromatolites

The results of temporal variation of sedimentary facies of global stromatolites are shown in Figure 7. At the era level in the Precambrian and the period level in geological time, the proportion of stromatolites found in shelf environments remained below 10%, except for a peak of 25% in the Mesoarchean and Siderian. Shoal stromatolites dominated, with proportions exceeding 50% except in the Siderian, Paleogene, and Quaternary periods, where proportions ranged from 30% to 46%. In the Archean, Paleoproterozoic,

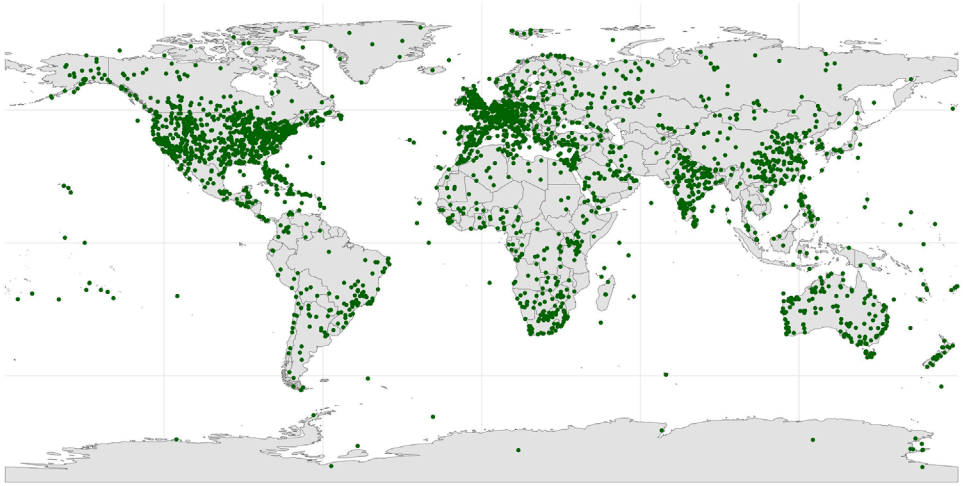

FIGURE 5
Global heat map of the modern locations of stromatolites. Repeat occurrences of the same stromatolite in multiple sources are excluded.

TABLE 3 The top ten countries with the highest frequency of occurrence.

Country	Occurrence
United States	853
Australia	197
India	180
Canada	180
China	169
United Kingdom	114
Russia	105
France	84
Spain	75
South Africa	72

and Mesoproterozoic, shoal stromatolites fluctuated but remained between 70% and 80% from the Neoproterozoic to the Devonian, with a peak of 86% in the Silurian, and varied between 30% and 70% from the Carboniferous to the Quaternary. Stromatolites inhabiting tidal environments remained relatively low (<18%), fluctuating between 12.5% and 0% in the Paleoproterozoic, increasing from 5% to 17% in the Mesoproterozoic, decreasing to 3%–5% in the Neoproterozoic, and fluctuating between 4.5% and 12.8% from the Cambrian to the Triassic before declining to less than 4.5% from the Jurassic to the Quaternary. The proportion of lagoon stromatolites remained below 10%, except for a peak of 12.5% in the Paleoarchean. Lagoon stromatolites were present in the Paleoarchean, Proterozoic (excluding the Rhyacian and Cryogenian), Cambrian-Ordovician, and Triassic-Neogene. Delta stromatolites appeared in the Rhyacian-Statherian of the Paleoproterozoic, Stenian-Cryogenian of the Mesoproterozoic-Neoproterozoic, Cambrian, Carboniferous-Permian, and Paleogene, with proportions less than 5% except for a peak of 7% in the Rhyacian and Cryogenian. Glacial stromatolites were present in the Orosirian of the Paleoproterozoic, Ectasian of the Mesoproterozoic, and three periods of the Neoproterozoic, as well as in the Cambrian, Carboniferous-Jurassic, and Paleogene periods, with proportions below 5% except for peaks of 6%–10% in the Ectasian, Tonian, and Cryogenian. Inland aquatic stromatolites were present at 10%–30% from the Mesoarchean to the Ectasian of the Mesoproterozoic, declined to 2%–7% in the Late Mesoproterozoic-Neoproterozoic, and remained at 2%–3% in the Early Paleozoic. They surged to 10%–30% in the Late Paleozoic, increased to 18%–40% in the Mesozoic, and remained high (40%–55%) in the Cenozoic. Notably, inland aquatic stromatolites were present at 10%–30% from the Devonian to the Jurassic and maintained high levels (39%–53%) from the Cretaceous to the Quaternary. This suggests a gradual migration of global stromatolites from marine to freshwater environments in the Late Mesozoic and Cenozoic, with a notable landward migration trend appearing since the Cretaceous.

4 Discussion

4.1 Abundance changes of global stromatolites

4.1.1 Similarities and differences between stromatolite occurrences and stromatolite-bearing stratigraphical units

Although there are differences in absolute values at the Period level, such as in the Quaternary, the overall trends in the records of stromatolite occurrences and stromatolite-bearing stratigraphic

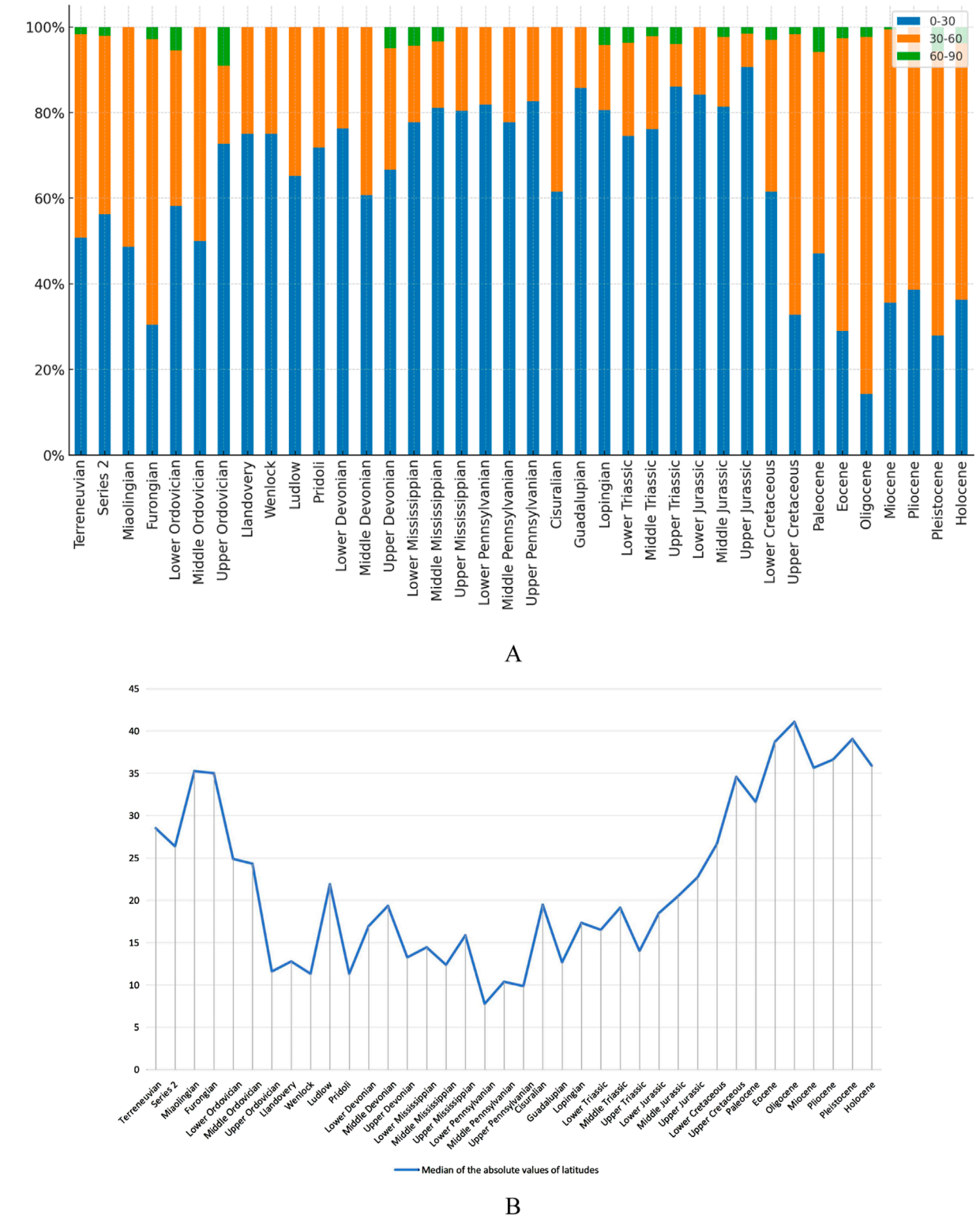

FIGURE 6
Paleolatitudinal distribution of stromatolites during the Phanerozoic. **(A)**Paleolatitudinal frequency distribution of stromatolites in each epoch. Data is divided into 30° paleolatitudinal bins. **(B)**The median paleolatitudes of all localities in each epoch.

units remain consistent. This consistency may be attributed to the longer timescale of data collection, which reduces sampling errors and ensures the coherence of the trends. The discrepancy observed in the Quaternary, where the abundance of stromatolite-bearing stratigraphic units is lower than that inferred from locality-age pairs, may be due to the lack of well-defined stratigraphic units

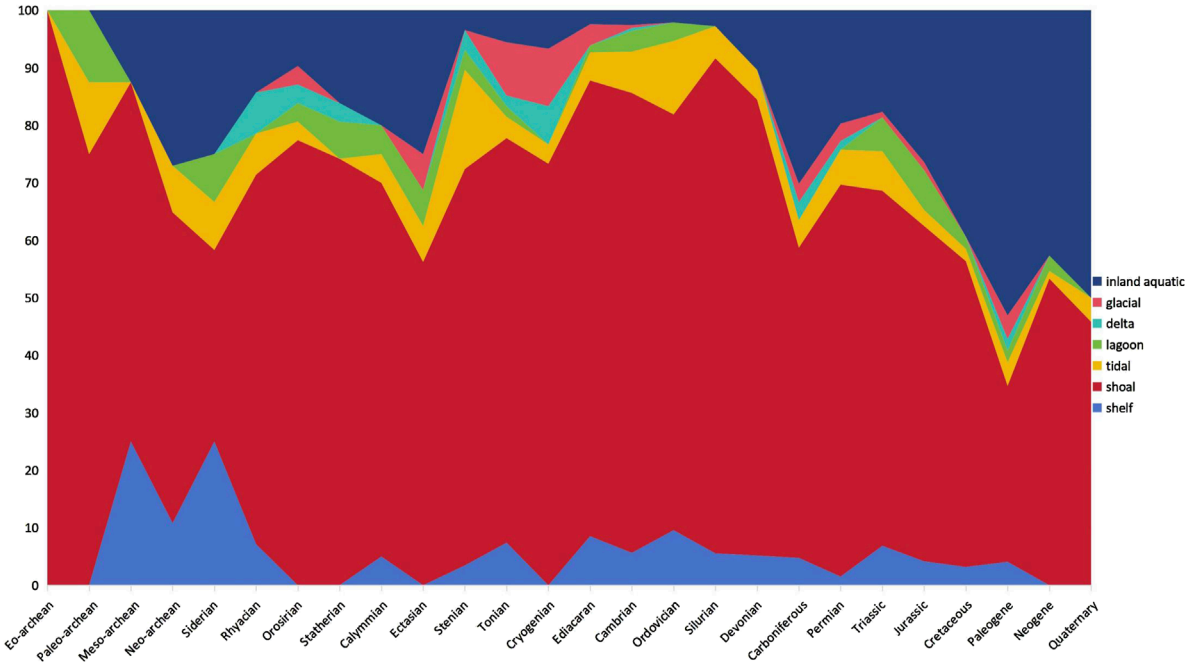

FIGURE 7
Proportional variations of global stromatolite occurrences in different facies (shelf, shoal, tidal, lagoon, delta, glacial, and inland aquatic) through geological time, based on the extraction of relational mentions of "stroma-age-facies" by ChatGPT-4.

for recent stromatolites. We calculated the Spearman correlation coefficient for the two parameters at the period level, which is approximately 0.437, with a p-value of 0.048, indicating a statistically significant positive correlation between the two variables.

At the age and epoch levels, to reduce potential sampling bias, we introduced a Normalization Index (NI), which is calculated using Equation 1.

$$NI = NS \div NT \quad (1)$$

NI: Normalization Index.

NS: Number of stromatolite-containing units.

NT: Total number of corresponding PBDB stratigraphic units for the period.

We present the NI and the occurrence of stromatolites in the figure below (Figure 8), where occurrence is on the left vertical axis and NI is on the right vertical axis.

At the age and epoch levels, despite differences in the intensity of research on stromatolites and the possibility that stromatolites from the same stratigraphic unit may be reported from multiple locations, which may lead to deviations in absolute values, especially at time points closer to the present, after normalization, we found that the trend of the normalized index (NI) is generally consistent with the frequency of stromatolite occurrences.

Similarly, we conducted a Spearman's test of NI and stromatolite occurrencesat at different levels. At the age level, the Spearman correlation coefficient is approximately 0.677, and the p-value is approximately 1.08×10^{-14}, indicating a statistically significant correlation between the two variables; at the epoch level, the Spearman correlation coefficient for the new data is approximately 0.615, and the p-value is approximately 6.49×10^{-5}, indicating a statistically significant moderate correlation between the two variables. The normalized trends and the stromatolite occurrence patterns showed significant consistency at different levels (Figure 8), further enhancing the reliability of the observed evolutionary signal. Overall, the trend of stromatolite abundance variation that we obtained reflects the real situation.

4.1.2 The relationship between stromatolite abundance and biodiversity, and dolomite in carbonates

Previous studies have suggested an inverse relationship between animal diversity and the abundance of microbialites, including stromatolites, during the Phanerozoic (Riding, 2005; Riding, 2006). Our study supports this view, revealing a weak negative correlation between animal genus-level diversity and stromatolite prevalence in carbonate-bearing rock units. This correlation is particularly noticeable in specific intervals, such as from the Guzhangian of the Middle Cambrian to the Pridoli of the Latest Silurian, and from the Frasnian of the Upper Devonian to the Serravallian of the Middle Neogene (Figure 4A).

The observed negative correlation between average metazoan genus-level diversity and stromatolite prevalence in carbonate-bearing rock units throughout much of the Phanerozoic may be attributed to several factors, including changes in ecological niches and competition, shifts in nutrient cycling and productivity, and variations in the marine chemical environment. Increased biodiversity may elevate competition between more complex

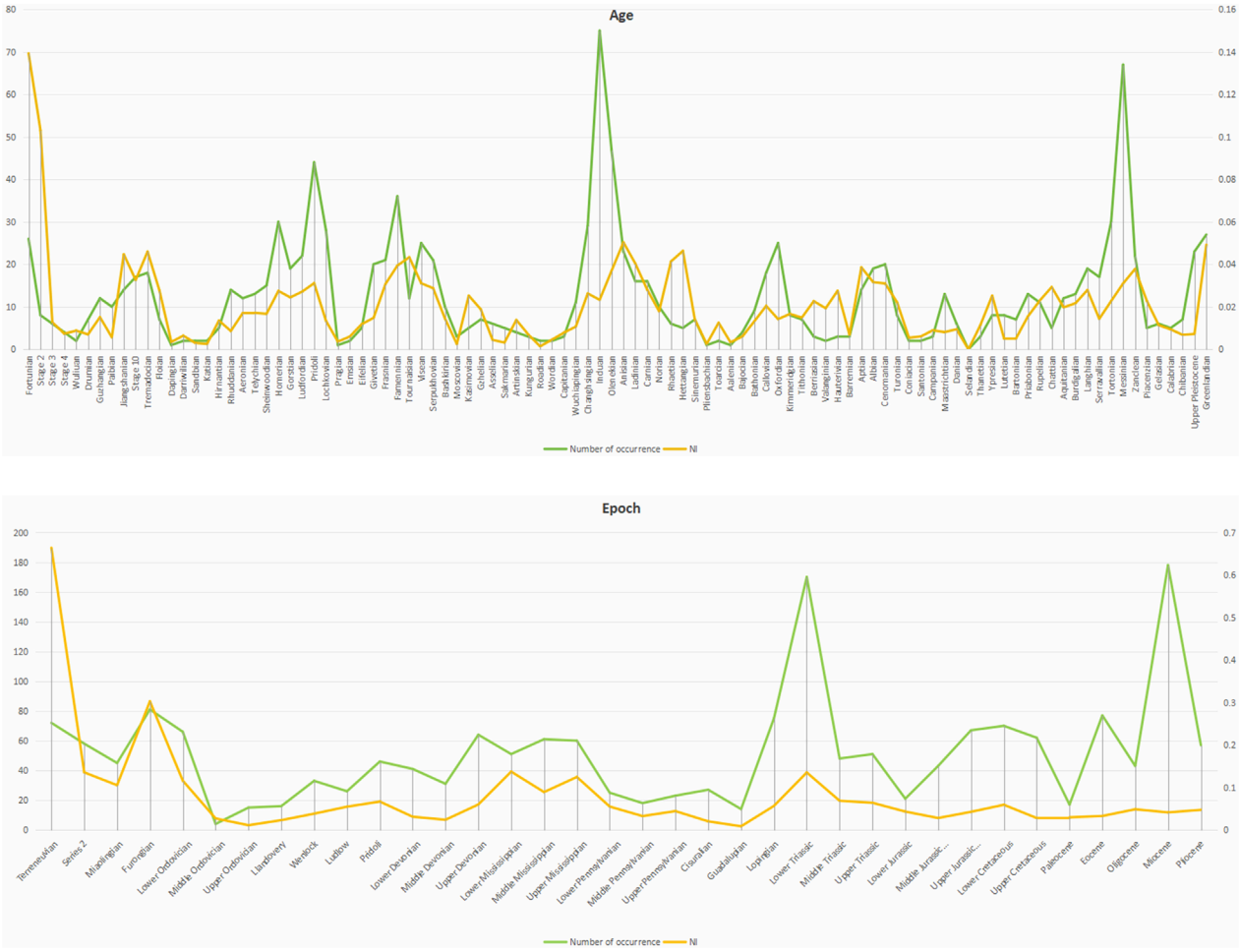

FIGURE 8
Occurrence and stratigraphic normalization index curves.

organisms and microorganisms for resources, potentially reducing the available niche for stromatolite-forming microorganisms such as cyanobacteria. As biodiversity rises, often accompanied by greater ecosystem complexity and resource efficiency, the likelihood of stromatolite formation may diminish, as a wider array of organisms could interfere with the development and maintenance of microbial mats (Riding, 2000). Stromatolite formation typically occurs in nutrient-rich environments, such as those high in phosphorus (Rao et al., 2000). An increase in plankton and benthic organisms may enhance the production and accumulation of organic matter, thereby altering trophic dynamics and potentially inhibiting stromatolite formation. Elevated biological productivity can result in increased sedimentation rates and a more dynamic sedimentary environment (Wood and Armitage, 1997; Le Hir et al., 2007), conditions which may not favor the stable environments necessary for stromatolite development. Additionally, changes in marine chemical conditions, such as variations in carbonate saturation and pH, may differently impact stromatolite formation and biodiversity.

There is a positive correlation between the proportion of dolomitic carbonate units and stromatolite-bearing carbonate units during certain intervals, specifically from the Fortunian in the early Cambrian to the Wuchiapingian of the Late Permian, and from the Hettangian in the early Jurassic to the Maastrichtian of the latest Cretaceous (Figure 4B). However, this correlation may be attenuated by the presence of at least two modes of dolomite formation: one occurring during the primary and early diagenetic stages, and the other during the late diagenetic stages of dolomitization in varying sedimentary environments.

The positive correlation between dolomitic carbonate units and stromatolite prevalence in carbonate-bearing rock units observed during certain periods of the Phanerozoic may be attributed to factors such as environmental stability, light conditions, sea level changes, and biogeochemical cycles. Relatively stable climates can create favorable conditions for stromatolite formation, particularly in shallow waters with high light levels and elevated temperatures. These conditions promote the proliferation of cyanobacteria, the primary biological components of stromatolites. Dolomite formation is often associated with higher calcium carbonate saturation and elevated water temperatures (Kell-Duivestein et al., 2019), which are prevalent in warm, shallow marine environments. Carbonate oversaturation can facilitate

the accumulation and preservation of microbial carbonates (Riding, 2000) and the formation of dolomites (Morse, 2003). Sea level fluctuations may influence nutrient distribution, biological community composition, and the development of extensive carbonate platforms, thereby impacting both stromatolite and dolomite formation. Additionally, changes in atmospheric and oceanic CO_2 concentrations can affect the global carbon cycle and carbonate deposition. Cyanobacterial photosynthesis contributes to local dolomite and stromatolite deposition, where such formations typically require lower sedimentation rates and reduced particulate matter input, conditions more easily met in warm, carbonate-saturated seawater environments. Moreover, extracellular polysaccharides in stromatolite-forming microbial mats may also promote dolomite formation (Zhang et al., 2012).

4.1.3 The reasons for changes in global stromatolite abundance

Stromatolites have exhibited significant fluctuations in abundance over the past 4 billion years, as evidenced by both stroma-strata-age and stroma-locality-age data. Although stromatolites have been reported from the Archean, including the Eoarchean (Figure 2), their scarcity may be due to early Earth's extreme conditions, such as harsh atmospheric and oceanic chemistry, low biodiversity, nascent microbial activity, and unstable sedimentary environments. Frequent volcanic activity and crustal movements (Hamilton, 1998; Liu et al., 2022) created unstable conditions, while fluctuating chemical compositions in oceans and lakes (Albarede et al., 2020) hindered biomat development. Moreover, low biodiversity and limited photosynthetic microorganisms capable of forming stromatolites (Allwood et al., 2009) contributed to their rarity. Ongoing debate surrounds whether some Archean structures resulted from biological activity (Nutman et al., 2016; Allwood et al., 2018).

The Proterozoic saw a rapid increase in stromatolites, attributed to the widespread distribution of cyanobacteria-dominated microbial communities. Stable ocean platforms, shallow water environments, large-scale carbonate deposition, oxygenation events, and low biological competition favored stromatolite formation. Cyanobacteria and other microorganisms thrived in the Proterozoic with relatively low-biodiversity (Sergeev et al., 2012), supporting stromatolite growth by facilitating calcium carbonate deposition through metabolic activity (Schirrmeister et al., 2013; Large et al., 2022; Baer, 1983).

Increased stromatolite prevalence in the Precambrian was due to minimal ecological competition, oxygen buildup, and stable sedimentary environments. Cyanobacteria's photosynthesis gradually increased atmospheric and oceanic oxygen levels (Schirrmeister et al., 2016), promoting microbial mat growth and stromatolite deposition.

During the Phanerozoic, reduced stromatolite abundance stemmed from increased biodiversity, predation pressures, ecological shifts, and changes in environmental and sedimentary conditions. Higher oxygen levels and the emergence of diverse biological groups limited niches for stromatolite-forming microorganisms, with predators disrupting microbial mats. As ecosystems became more complex, available niches for stromatolite builders shrank.

Stromatolite abundance during the Fortunian stage of the Cambrian was driven by low biodiversity, reduced ecological competition, the development of carbonate platforms, and stable marine conditions. Microorganisms, particularly photosynthetic bacteria (Cui et al., 2020), thrived in this ecosystem, forming stromatolites in stable shallow marine environments. The high abundance of stromatolites in carbonate deposits during the Terreneuvian and Furongian epochs of the Cambrian can be linked to ecological competition, niche adaptation, and widespread carbonate platforms (Zhang et al., 2016; Riaz et al., 2019). Primitive microbial mats continued to occupy ecological niches in shallow seas, with increased oxygen and nutrient circulation promoting stromatolite formation. In the Tremadocian stage of the Ordovician, factors such as ecological competition, niche preservation, and the development of carbonate platforms contributed to stromatolite abundance. Despite multicellular organisms becoming dominant, stromatolite-forming microorganisms thrived in specific environments with high salinity or extreme pH (Wang et al., 2021).

In the Pridoli stage of the Silurian, global sea level rises, warm climates, flourishing marine ecosystems, and anoxic events played a role in stromatolite formation (Vacek et al., 2018; Kaminskas et al., 2015; Vandenbroucke et al., 2015). The rise in sea levels expanded marine environments, while warm conditions promoted organism growth, contributing to organic carbonate deposits. Marine anoxic events further preserved organic carbonates and stromatolite structures. During the Famennian stage of the Late Devonian, climatic fluctuations, extensive marine environments, and anoxic events facilitated stromatolite formation. Sea level fluctuations and sediment transport contributed to stromatolite deposits, while reef-building organisms and marine anoxic events aided in preserving organic carbonates (Bond and Wignall, 2008; Zhang et al., 2020).

In the Visean stage of the Lower Carboniferous, favorable climatic conditions, high sea levels, and extensive carbonate platforms supported the formation of stromatolites (Pfefferkorn et al., 2014; Yao et al., 2016; Somerville et al., 2009). Warm, wet conditions provided stable shallow water environments for microorganism photosynthesis, further facilitating stromatolite formation.

In the Early Triassic's Induan stage, post-extinction recovery and new ecological niches led to stromatolite proliferation in stable shallow water environments, aided by volcanic activity altering ocean chemistry (Chen and Xu, 2019; Cui et al., 2021; Kershaw et al., 2011; Wang et al., 2019). The peak in stromatolite prevalence during the Early Triassic, as previously noted (Schubert and Bottjer, 1992), aligns with the high proportion of stromatolite-bearing rocks in carbonate formations of the Induan stage (Mary and Woods, 2008)[-] (Fang et al., 2017). Stromatolite abundance during the Late Triassic's Carnian stage was driven by the Carnian Pluvial Event (Simms and Ruffell, 2018), creating favorable conditions for microbial mat formation.

The Oxfordian stage of the Late Jurassic saw stromatolites thrive in greenhouse climates, extensive shallow marine environments, and stable biogeochemical processes, supported by high sea levels and optimal light conditions (Price and Rogov, 2009; Olivier et al., 2004; Louis-Schmid et al., 2007).

The Cretaceous and Miocene periods also witnessed stromatolite peaks due to greenhouse climates, high sea levels,

and extensive carbonate platform development (Lü et al., 2013; Shao et al., 2017; Huber et al., 2018; Tierney et al., 2019; Dumitru et al., 2019; Pohl et al., 2020; Steinthorsdottir et al., 2021; Wei and Tian, 2022). The extreme salinity in the Messinian stage at the end of the Miocene in the Mediterranean favored cyanobacteria, enhancing stromatolite formation. Climatic shifts and geographical changes may have also influenced stromatolite distribution during this period (Kontakiotis et al., 2022; Krijgsman et al., 2024; Simon and Meijer, 2017; Vasiliev et al., 2017; Leroux et al., 2018).

During the Pleistocene, frequent climate changes and sea level fluctuations promoted microbial activity and stromatolite formation, with enhanced nutrient availability during interglacial periods (Chalk et al., 2017; Willeit et al., 2019; Yamamoto et al., 2022). The climatic fluctuations, local environmental conditions, and human impacts in the Meghalayan stage further facilitated stromatolite growth (Carvalho et al., 2018; Martin-Bello et al., 2019; Yue and Gao, 2018; Piotrowska et al., 2020). Similarly, the Holocene saw increased stromatolite-bearing rocks due to climate stability, rising sea levels, and human influence (Xiong et al., 2018; Shtienberg et al., 2022; Bader et al., 2020; Kaufman and Broadman, 2023).

4.2 Locality and latitude distributions of global stromatolites

Stromatolites were particularly abundant in North America, where numerous shallow marine and lacustrine environments provide ideal conditions for their formation. The relatively stable climate in parts of North America over long geological periods has favored the growth and preservation of stromatolites. Additionally, the region's suitable sedimentary environments, well-preserved strata, and extensive scientific research have contributed to the high abundance of stromatolites in North America (Peters et al., 2017).

Stromatolites are widely distributed in many regions around the world, including the United States, Australia, India, Canada, China, the United Kingdom, and Russia. Although the environmental conditions in these regions vary, they share some common characteristics that provide ideal conditions for the formation and preservation of stromatolites. The warm climate, shallow seas and lake environments, and high carbonate sedimentation rates in the United States are favorable for the development of stromatolites. Warm and clear shallow seas, low salinity water, and high sedimentation rates in Australia also promote the growth of stromatolites. India features stable shallow marine environments and suitable climate conditions. In Canada, China, and Russia, stromatolites predominantly develop in specific sedimentary environments such as lakes, tidal flats, or shallow seas, with low hydrodynamic conditions and high carbonate sedimentation rates. In the United Kingdom, ancient sedimentary rocks have stable geological environments and good fossil preservation conditions, with stromatolites mainly forming in shallow marine or lake environments. Low hydrodynamic conditions and high sedimentation rates contribute to their formation. Overall, the common favorable features of these regions include shallow water environments, clear waters, low hydrodynamic conditions, high carbonate sedimentation rates, and climates conducive to microbial growth, which provide ideal natural conditions for the growth and preservation of stromatolites.

Most stromatolites were distributed in low and middle latitudes during the Phanerozoic. The warm climate and extensive shallow marine environments in these regions created ideal conditions for microorganisms and stromatolite growth. The seawater in low and middle latitudes is typically clear, with moderate salinity and ample light, which facilitates photosynthesis and microbial activity, thereby supporting the formation of stromatolites.

The shift in the distribution of stromatolites from lower paleolatitudes (0°–30°) to higher paleolatitudes (30°–60°), as evidenced by the higher median paleolatitudes of stromatolite localities from the Cretaceous to the Quaternary, suggests a migration toward higher latitudes during this period. Since the Cretaceous, Earth has undergone significant climate changes, including global warming periods, which have rendered cooler mid-to-high latitudes more favorable for microbial life, particularly cyanobacteria responsible for stromatolite formation. Tectonic plate movements have altered continental positions, causing some regions previously situated at low latitudes to migrate toward middle and high latitudes, thus introducing new stromatolite distribution patterns (Scotese et al., 2025). Fluctuations in global sea levels and shifts in ocean currents have further influenced the stability and distribution of marine environments (Sames et al., 2016). Mid-to-high latitudes have potentially emerged as new microbial habitats due to ocean currents delivering increased nutrients and stabilizing water temperatures (Rautio et al., 2008; Griffis and Howard, 2013). As plant and animal diversity expanded in the oceans, stromatolite-forming cyanobacteria and other microorganisms encountered intensified competitive pressures. This increased competition, coupled with predation in lower latitudes, may have driven these microbes to seek refuge in cooler, less competitive mid-to-high latitudes. Additionally, long-term global climate change has possibly extended the habitable zones of the tropics and subtropics poleward, enhancing the suitability of middle and high latitudes for stromatolite formation. Collectively, these factors have allowed stromatolites to inhabit a broader range of geographical locations from the Cretaceous to the Quaternary period.

4.3 Temporal variation of sedimentary facies of global stromatolites

Throughout the Precambrian and various periods of the Phanerozoic in geological history, stromatolites in shelf environments have generally constituted less than 10% of the total, with notable exceptions in the Mesoarchean and Siderian, where the proportion reached 25%. This low proportion is due to several factors. Some shelf areas may be too deep for effective photosynthesis, limiting stromatolite formation. Shelf regions typically accumulate river-transported sediments (Wheatcroft and Sommerfield, 2005; Gao and Collins, 2014), and high sedimentation rates can physically destroy microbial mats and bury stromatolite-forming communities. Additionally, strong currents can alter sedimentary environments, erode sediments (Harris, 2014; Vieira et al., 2019), and disrupt microbial mat development. The high biodiversity in shelf regions (Teichert, 2014; Brasier et al., 2018; Alabia et al., 2021) also increases

ecological competition and predation pressure on stromatolite-forming microorganisms. The hydrochemical conditions on shelves may be less favorable, with elevated nutrient salt concentrations (Guo et al., 2020; Flynn et al., 2020) promoting biomass growth that competes with stromatolite-associated microbial communities.

The abundant stromatolites in shelf environments during the Mesoarchean and Siderian are attributed to factors like increased oxygen levels, favorable water conditions, low biological competition, global sea level changes, climate stability, and chemical deposition processes. During the Siderian period, the Great Oxidation Event significantly raised atmospheric oxygen, allowing oxygen-dependent organisms like cyanobacteria to thrive (Gumsley et al., 2017; Warke et al., 2020). Cyanobacteria, key architects of stromatolites, proliferated, and the shallow, well-lit waters of the Mesoarchean and Siderian provided ideal conditions for photosynthesis. The absence of complex multicellular organisms allowed cyanobacteria to dominate. Global sea level rise and stable climate conditions facilitated the expansion of shallow marine environments conducive to stromatolite growth. The abundance of iron in the oceans during the Siderian (Beukes and Gutzmer, 2008) supported microbial activity and promoted stromatolite formation.

Stromatolites in shoal environments are abundant due to several favorable conditions: shallow depths, abundant sunlight, stable substrates, clear water, suitable hydrodynamics, and reduced biological competition. These factors promote the development and preservation of stromatolites. Shoals provide optimal conditions for cyanobacteria growth, the primary builders of stromatolites (Zhou et al., 2014), as the stable sediment is less prone to erosion (Harris et al., 2012; Trower et al., 2018). Clear water minimizes the obstruction of photosynthesis, and high levels of carbonates and other minerals (Dalrymple and Rivers, 2023) facilitate calcium carbonate deposition. Shoal environments also experience lower biological competition, allowing microbial communities to thrive with minimal pressure.

The scarcity of stromatolites in tidal environments is due to challenging factors like strong hydrodynamic activity, rapid sediment deposition and erosion, frequent tidal fluctuations, turbid water quality, unstable chemical conditions, ecological competition, and bioturbation. Strong currents and sediment transport in tidal areas (Wright, 1977; Zhang et al., 2018; Ridderinkhof, 2019) can erode or bury microbial mats. Tidal action often results in water bodies laden with suspended particles (Winter et al., 2007; Ahn, 2012), which diminish the photosynthetic efficiency of the microorganisms that construct stromatolites. The chemical environment in tidal zones may change frequently due to tidal fluctuations and rainfall (Ovalle et al., 1990). Turbid waters reduce photosynthesis efficiency, and tidal fluctuations alter water depth (Devlin et al., 2017), affecting microbial mat stability. High biodiversity in tidal ecosystems (Yoo et al., 2013; De Santana et al., 2021) increases competition and bioturbation, disrupting stromatolite formation.

Lagoons, while having some conditions that promote microbial growth (higher nutrient levels), suffer from several adverse factors, including poor water quality, turbidity, insufficient light, ecological competition, bioturbation, unstable chemical environments, and unsuitable sediments. Lagoons often have hypoxic conditions and high salinity (Franco et al., 2019; Hsieh et al., 2021), which are unfavorable for oxygen-dependent, photosynthetic microbes. The turbidity of lagoon water (Obrador and Pretus, 2008; Sebastiá-Frasquet et al., 2019) limits light penetration, and high biodiversity (Bellino et al., 2019; Giampaoletti et al., 2023) leads to competition with stromatolite-forming microbes for light and nutrients. The enclosed nature of lagoons makes them vulnerable to land runoff, which can rapidly alter hydrochemical conditions (Chagas and Suzuki, 2005). Additionally, the loose sediments in lagoons are not conducive to stromatolite consolidation and growth (Calliari et al., 2009; Schubert and Telesh, 2017).

In delta environments, the rapid deposition rates, dynamic water flows, turbid waters, and fluctuations in chemical and nutrient conditions hinder stromatolite formation. Rivers transport significant sediment to deltas, which quickly buries and inhibits stromatolite growth (Besset et al., 2019; Hori and Saito, 2022). The dynamic conditions created by both river and tidal forces (Hoitink et al., 2017) disrupt stromatolite formation, and the turbid water limits light penetration, adversely affecting photosynthetic microorganisms. The input of nutrients from land runoff (Zhang et al., 2021) encourages other microbial growth, further competing with stromatolite-forming microorganisms. Additionally, the high biodiversity in deltas (Rakib et al., 2022) includes numerous benthic animals that can disturb or destroy microbial mats, further hindering stromatolite formation.

Glacial environments are not conducive to stromatolite formation due to extreme low temperatures that inhibit bacterial metabolism (Stibal et al., 2012), especially among cyanobacteria. Snow and ice reflect sunlight (Perovich et al., 2008), reducing light availability for photosynthetic microorganisms. Glacial sediments are often coarse and do not provide stable substrates for microbial mats (Jehu, 1909). Additionally, meltwater lacks the nutrients necessary for microbial growth and stromatolite formation, and glacier dynamics, including pushing and abrasion (Alley et al., 2019), can destroy microbial mats, further hindering stromatolite formation.

From the Mesoarchean to the Ectasian of the Mesoproterozoic, stromatolites in inland aquatic environments were notably high due to continental expansion, climate and sea level changes, low biological competition, changes in the chemical environment, and terrestrial geological processes. Significant continental growth and stabilization (Zhai et al., 2020; Cawood et al., 2022) created suitable environments for microbial mats in shallow lakes, rivers, and lagoons. Climatic fluctuations caused sea levels to rise and fall (Eriksson et al., 2005), exposing vast areas of shallow water, ideal for stromatolite formation. Low biodiversity (Knoll et al., 2006; Stüeken and Buick, 2018) reduced ecological competition, and rising oxygen levels (Lyons et al., 2014) further influenced microbial growth. Terrestrial geological processes like volcanic activity (Agangi et al., 2020) provided nutrients, promoting stromatolite distribution.

From the mid-Mesoproterozoic to Early Paleozoic, stromatolite abundance decreased in inland aquatic environments due to increased biodiversity, atmospheric and oceanic oxidation, plant evolution, climate changes, and sedimentary environment changes. The emergence of multicellular algae and plants (Planavsky et al., 2015; Porter and Riedman, 2023) directly competed with stromatolite-forming microorganisms. The terrestrial oxidation event (Och and Shields-Zhou, 2012) increased oxygen levels, inhibiting anaerobic microorganisms crucial for stromatolite formation. The evolving ecosystem, changes in chemical deposition

processes, and plant activities altered the sedimentary environment (Dahl and Arens, 2020)' challenging stromatolite formation. Major climate changes and sea level fluctuations may have contributed to the instability of continental environments (Haq and Schutter, 2008; Nardin et al., 2011; Marcilly et al., 2022), such as frequent droughts and floods, negatively impacting the environment for stromatolite formation. The drift of continental plates and geological tectonic activity (Domeier, 2018) led to the formation of new mountains and basins, creating sedimentary environments unsuitable for stromatolite formation, such as deep water basins or rapidly eroding mountainous areas. These factors combined to limit stromatolite formation in continental environments during the mid-Mesoproterozoic to Early Paleozoic.

In the Devonian to Jurassic periods, inland aquatic stromatolites increased due to the stability of continental environments, favorable climate conditions, and reduced biological competition. The expansion and stabilization of continental environments (Golonka, 2020) provided ideal shallow-water environments for stromatolite formation. Seasonal lakes and arid regions allowed cyanobacteria to flourish in low-competition areas (Arenas et al., 2015; Silveira et al., 2023). Sea level changes (Jank et al., 2006; Kabanov et al., 2023) also created temporary shallow-water environments conducive to stromatolite formation, and the diversification of terrestrial plants and animals (Davis and Matthews, 2019; Close et al., 2019) indirectly supported microbial communities.

During the Cretaceous to Quaternary periods, the high proportion of stromatolites in inland aquatic environments resulted from climatic conditions, biological evolution, ecosystem changes, and enhanced chemical deposition. Warm climates and elevated CO_2 levels in the Cretaceous (Huber et al., 2018) led to shallow, warm water environments ideal for stromatolite formation. Despite increased biodiversity, certain geological periods and environments (e.g., polar regions) experienced reduced biological competition, allowing stromatolite formation. Glacial activity in the Quaternary led to the formation of glacial lakes, which became hotspots for microbial activity and stromatolite formation (Petryshyn et al., 2016). Sea level changes exposed large land areas, providing new environments for stromatolite formation (Ray et al., 2019). Interglacial periods with warm and humid conditions stabilized some lakes, further promoting stromatolite growth (McCall, 2010).

5 Conclusions and future works

The application of the ChatGPT-4 large language model technique has proven to be an effective tool for extracting geological information from scientific literature. The newly developed knowledge base of global stromatolite occurrences reveals several key trends: stromatolite occurrences were relatively low during the Archean, experienced a sustained increase throughout the Proterozoic, sharply declined at the Cambrian-Ordovician boundary, and underwent frequent fluctuations after the Silurian. The United States, Australia, India, Canada, China, England, and Russia have been identified as the seven major hotspots for stromatolite records. From the Cambrian to the Jurassic, stromatolites were primarily distributed in low and middle latitudes, but from the Cretaceous to the Quaternary, they shifted to higher latitudes. Analysis of stromatolite versus facies data indicates that the proportions of inland aquatic stromatolites were 10%–30% from the Mesoarchean to the Middle Mesoproterozoic, decreased to 2%–7% from the Late Mesoproterozoic to the Early Paleozoic, rose again to 10%–30% during the Devonian to Jurassic, and maintained high levels (39%–53%) from the Cretaceous to the Quaternary.

As a novel text mining approach, ChatGPT-4 demonstrates significant potential for advancing knowledge discovery in sedimentology. In future research, applying this methodology to investigate the stratigraphic abundance and paleogeographic distribution of other distinctive sedimentary structures, such as thrombolites, ooids, oncoids, and leiolites, could enhance our understanding of biological and environmental changes throughout geological time. However, due to current technological limitations, it is still challenging to fully and accurately extract information from charts, tables, and images. Therefore, this paper does not address the extraction of such data. We plan to attempt solving this issue in future research and have included it in our future work.

Data availability statement

The datasets presented in this study can be found in online repositories. The names of the repository/repositories and accession number(s) can be found in the article/supplementary material.

Author contributions

HL: Writing–original draft. MZ: Writing–review and editing.

Funding

The author(s) declare that financial support was received for the research and/or publication of this article. This work was supported by three grants from the Hubei Provincial Construction Science and Technology Plan Project for the Year 2024 (JK2024127) and doctoral fund of Huanggang Normal University (2024085) and high-level nurturing program project of Huanggang Normal University (202424504).

Conflict of interest

The authors declare that the research was conducted in the absence of any commercial or financial relationships that could be construed as a potential conflict of interest.

Generative AI statement

The author(s) declare that no Generative AI was used in the creation of this manuscript.

Publisher's note

All claims expressed in this article are solely those of the authors and do not necessarily represent those of their affiliated

organizations, or those of the publisher, the editors and the reviewers. Any product that may be evaluated in this article, or claim that may be made by its manufacturer, is not guaranteed or endorsed by the publisher.

References

Agangi, A., Hofmann, A., Hegner, E., Xie, H., Teschner, C., Slabunov, A., et al. (2020). The Mesoarchaean Dominion Group and the onset of intracontinental volcanism on the Kaapvaal craton–geological, geochemical and temporal constraints. *Gondwana Res.* 84, 131–150. doi:10.1016/j.gr.2020.03.005

Ahn, J. H. (2012). Size distribution and settling velocities of suspended particles in a tidal embayment. *Water Res.* 46 (10), 3219–3228. doi:10.1016/j.watres.2012.03.038

Alabia, I. D., García Molinos, J., Hirata, T., Mueter, F. J., Hirawake, T., and Saitoh, S. (2021). Marine biodiversity refugia in a climate-sensitive subarctic shelf. *Glob. change Biol.* 27 (14), 3299–3311. doi:10.1111/gcb.15632

Albarede, F., Thibon, F., Blichert-Toft, J., and Tsikos, H. (2020). Chemical archeoceanography. *Chem. Geol.* 548, 119625. doi:10.1016/j.chemgeo.2020.119625

Alley, R. B., Cuffey, K. M., and Zoet, L. K. (2019). Glacial erosion: status and outlook. *Ann. Glaciol.* 60 (80), 1–13. doi:10.1017/aog.2019.38

Allwood, A. C., Grotzinger, J. P., Knoll, A. H., Burch, I. W., Anderson, M. S., Coleman, M. L., et al. (2009). Controls on development and diversity of Early Archean stromatolites. *Proc. Natl. Acad. Sci.* 106 (24), 9548–9555. doi:10.1073/pnas.0903323106

Allwood, A. C., Rosing, M. T., Flannery, D. T., Hurowitz, J. A., and Heirwegh, C. M. (2018). Reassessing evidence of life in 3,700-million-year-old rocks of Greenland. *Nature* 563 (7730), 241–244. doi:10.1038/s41586-018-0610-4

Arenas, C., Piñuela, L., and García-Ramos, J. C. (2015). Climatic and tectonic controls on carbonate deposition in syn-rift siliciclastic fluvial systems: a case of microbialites and associated facies in the Late Jurassic. *Sedimentology* 62 (4), 1149–1183. doi:10.1111/sed.12182

Babilonia, J., Conesa, A., Casaburi, G., Pereira, C., Louyakis, A. S., Reid, R. P., et al. (2018). Comparative metagenomics provides insight into the ecosystem functioning of the Shark Bay Stromatolites, Western Australia. *Front. Microbiol.* 9, 1359. doi:10.3389/fmicb.2018.01359

Bader, J., Jungclaus, J., Krivova, N., Lorenz, S., Maycock, A., Raddatz, T., et al. (2020). Global temperature modes shed light on the Holocene temperature conundrum. *Nat. Commun.* 11 (1), 4726. doi:10.1038/s41467-020-18478-6

Baer, A. J. (1983). Proterozoic orogenies and crustal evolution. *Geol. Soc. Am. Memoirs* 161, 47–58. doi:10.1130/mem161-p47

Bellino, A., Mangano, M. C., Baldantoni, D., Russell, B. D., Mannino, A. M., Mazzola, A., et al. (2019). Seasonal patterns of biodiversity in Mediterranean coastal lagoons. *Divers. Distributions* 25 (10), 1512–1526. doi:10.1111/ddi.12942

Besset, M., Anthony, E. J., and Bouchette, F. (2019). Multi-decadal variations in delta shorelines and their relationship to river sediment supply: an assessment and review. *Earth-science Rev.* 193, 199–219. doi:10.1016/j.earscirev.2019.04.018

Beukes, N. J., and Gutzmer, J. (2008). Origin and paleoenvironmental significance of major iron formations of the archean-paleoproterozoic boundary. *Rev. Econ. Geol.* 15, 5–47. doi:10.5382/rev.15.01

Bond, D. P. G., and Wignall, P. B. (2008). The role of sea-level change and marine anoxia in the Frasnian–Famennian (Late Devonian) mass extinction. *Palaeogeogr. Palaeoclimatol. Palaeoecol.* 263 (3-4), 107–118. doi:10.1016/j.palaeo.2008.02.015

Brasier, M. J., Grant, S. M., Trathan, P. N., Allcock, L., Ashford, O., and Blagbrough, H. (2018). Benthic biodiversity in the South Orkney Islands Southern shelf marine protected area. *Biodiversity* 19 (1-2), 5–19. doi:10.1080/14888386.2018.1468821

Cahyana, D., Hadiarto, A., Hati, D. P., Pratamaningsih, M. M., Karolinoerita, V., Mulyani, A., et al. (2024). Application of ChatGPT in soil science research and the perceptions of soil scientists in Indonesia. *Artif. Intell. Geosciences* 5, 100078. doi:10.1016/j.aiig.2024.100078

Calliari, L. J., Winterwerp, J. C., Fernandes, E., Cuchiara, D., Vinzon, S., Sperle, M., et al. (2009). Fine grain sediment transport and deposition in the Patos Lagoon–Cassino beach sedimentary system. *Cont. Shelf Res.* 29 (3), 515–529. doi:10.1016/j.csr.2008.09.019

Cantine, M. D., Knoll, A. H., and Bergmann, K. D. (2020). Carbonates before skeletons: a database approach. *Earth-Science Rev.* 201, 103065. doi:10.1016/j.earscirev.2019.103065

Carvalho, C., Oliveira, M. I. N., Macario, K., Guimarães, R. B., Keim, C. N., Sabadini-Santos, E., et al. (2018). Stromatolite growth in Lagoa Vermelha, southeastern coast of Brazil: evidence of environmental changes. *Radiocarbon* 60 (2), 383–393. doi:10.1017/rdc.2017.126

Cawood, P. A., Chowdhury, P., Mulder, J. A., Hawkesworth, C. J., Capitanio, F. A., Gunawardana, P. M., et al. (2022). Secular evolution of continents and the Earth system. *Rev. Geophys.* 60 (4), e2022RG000789. doi:10.1029/2022rg000789

Chagas, G. G., and Suzuki, M. S. (2005). Seasonal hydrochemical variation in a tropical coastal lagoon (Açu Lagoon, Brazil). *Braz. J. Biol.* 65, 597–607. doi:10.1590/s1519-69842005000400006

Chalk, T. B., Hain, M. P., Foster, G. L., Rohling, E. J., Sexton, P. F., Badger, M. P. S., et al. (2017). Causes of ice age intensification across the Mid-Pleistocene Transition. *Proc. Natl. Acad. Sci.* 114 (50), 13114–13119. doi:10.1073/pnas.1702143114

Chen, J., and Xu, Y. (2019). Establishing the link between Permian volcanism and biodiversity changes: insights from geochemical proxies. *Gondwana Res.* 75, 68–96. doi:10.1016/j.gr.2019.04.008

Close, R. A., Benson, R. B. J., Alroy, J., Behrensmeyer, A. K., Benito, J., Carrano, M. T., et al. (2019). Diversity dynamics of Phanerozoic terrestrial tetrapods at the local-community scale. *Nat. Ecol. and Evol.* 3 (4), 590–597. doi:10.1038/s41559-019-0811-8

Cui, L., Liu, W., and Zhang, X. (2020). Phosphatized microbial fossils from the lowest Cambrian of South China and their ecological and environmental implications for the Kuanchuanpu biota. *Precambrian Res.* 338, 105560. doi:10.1016/j.precamres.2019.105560

Cui, Y., Li, M., Van Soelen, E. E., Peterse, F., and Kürschner, W. M. (2021). Massive and rapid predominantly volcanic CO2 emission during the end-Permian mass extinction. *Proc. Natl. Acad. Sci.* 118 (37), e2014701118. doi:10.1073/pnas.2014701118

Dahl, T. W., and Arens, S. K. M. (2020). The impacts of land plant evolution on Earth's climate and oxygenation state–An interdisciplinary review. *Chem. Geol.* 547, 119665. doi:10.1016/j.chemgeo.2020.119665

Dalrymple, R. W., and Rivers, J. M. (2023). A new look at modern carbonate shoals and coastal barrier systems. *Earth-Science Rev.* 246, 104553. doi:10.1016/j.earscirev.2023.104553

Davis, C. C., and Matthews, S. (2019). *Evolution of land plants*. New York: Oxford University Press.

De Santana, C. O., Spealman, P., Melo, V. M. M., Gresham, D., de Jesus, T. B., and Chinalia, F. A. (2021). Effects of tidal influence on the structure and function of prokaryotic communities in the sediments of a pristine Brazilian mangrove. *Biogeosciences* 18 (7), 2259–2273. doi:10.5194/bg-18-2259-2021

Devlin, A. T., Jay, D. A., Zaron, E. D., Talke, S. A., Pan, J., and Lin, H. (2017). Tidal variability related to sea level variability in the Pacific Ocean. *J. Geophys. Res. Oceans* 122 (11), 8445–8463. doi:10.1002/2017jc013165

Domeier, M. (2018). Early Paleozoic tectonics of Asia: towards a full-plate model. *Geosci. Front.* 9 (3), 789–862. doi:10.1016/j.gsf.2017.11.012

Dumitru, O. A., Austermann, J., Polyak, V. J., Fornós, J. J., Asmerom, Y., Ginés, J., et al. (2019). Constraints on global mean sea level during Pliocene warmth. *Nature* 574 (7777), 233–236. doi:10.1038/s41586-019-1543-2

Eriksson, P. G., Catuneanu, O., Sarkar, S., and Tirsgaard, H. (2005). Patterns of sedimentation in the precambrian. *Sediment. Geol.* 176 (1-2), 17–42. doi:10.1016/j.sedgeo.2005.01.003

Fang, Y., Chen, Z. Q., Kershaw, S., Li, Y., and Luo, M. (2017). An early triassic (smithian) stromatolite associated with giant ooid banks from lichuan (Hubei province), South China: environment and controls on its formation. *Palaeogeogr. Palaeoclimatol. Palaeoecol.* 486, 108–122. doi:10.1016/j.palaeo.2017.02.006

Flynn, R. F., Granger, J., Veitch, J. A., Siedlecki, S., Burger, J. M., Pillay, K., et al. (2020). On-shelf nutrient trapping enhances the fertility of the southern Benguela upwelling system. *J. Geophys. Res. Oceans* 125 (6), e2019JC015948. doi:10.1029/2019jc015948

Franco, T. P., Neves, L. M., and Araújo, F. G. (2019). Better with more or less salt? The association of fish assemblages in coastal lagoons with different salinity ranges. *Hydrobiologia* 828, 83–100. doi:10.1007/s10750-018-3804-8

Fuchs, A., Trachsel, T., Weiger, R., and Eggmann, F. (2024). ChatGPT's performance in dentistry and allergyimmunology assessments: a comparative study. *Swiss Dendal J. SSO–Science Clin. Top.* 134 (2), 1–17. doi:10.61872/sdj-2024-06-01

Gao, S., and Collins, M. B. (2014). Holocene sedimentary systems on continental shelves. *Mar. Geol.* 352, 268–294. doi:10.1016/j.margeo.2014.03.021

Giampaoletti, J., Sbrana, A., Magni, P., and Gravina, M. F. (2023). Macrobenthos of the tortolì lagoon: a peculiar case of high benthic biodiversity among mediterranean lagoons. *Diversity* 15 (6), 783. doi:10.3390/d15060783

Golonka, J. (2020). Late Devonian paleogeography in the framework of global plate tectonics. *Glob. Planet. Change* 186, 103129. doi:10.1016/j.gloplacha.2020.103129

Griffis, R., and Howard, J. (2013). *Oceans and marine resources in a changing climate: a technical input to the 2013 national climate assessment[M]*. Washington, DC: Island Press.

Gumsley, A. P., Chamberlain, K. R., Bleeker, W., Söderlund, U., de Kock, M. O., Larsson, E. R., et al. (2017). Timing and tempo of the great oxidation event. *Proc. Natl. Acad. Sci.* 114 (8), 1811–1816. doi:10.1073/pnas.1608824114

Guo, C., Zhang, G., Sun, J., Leng, X., Xu, W., Wu, C., et al. (2020). Seasonal responses of nutrient to hydrology and biology in the southern Yellow Sea. *Cont. Shelf Res.* 206, 104207. doi:10.1016/j.csr.2020.104207

Hamilton, W. B. (1998). Archean tectonics and magmatism. *Int. Geol. Rev.* 40 (1), 1–39. doi:10.1080/00206819809465196

Haq, B. U., and Schutter, S. R. (2008). A chronology of Paleozoic sea-level changes. *Science* 322 (5898), 64–68. doi:10.1126/science.1161648

Harris, B. P., Cowles, G. W., and Stokesbury, K. D. E. (2012). Surficial sediment stability on georges bank, in the great South channel and on eastern nantucket shoals. *Cont. Shelf Res.* 49, 65–72. doi:10.1016/j.csr.2012.09.008

Harris, P. T. (2014). Shelf and deep-sea sedimentary environments and physical benthic disturbance regimes: a review and synthesis. *Mar. Geol.* 353, 169–184. doi:10.1016/j.margeo.2014.03.023

Hohl, S. V., and Viehmann, S. (2021). Stromatolites as geochemical archives to reconstruct microbial habitats through deep time: potential and pitfalls of novel radiogenic and stable isotope systems. *Earth-Science Rev.* 218, 103683. doi:10.1016/j.earscirev.2021.103683

Hoitink, A. J. F., Wang, Z. B., Vermeulen, B., Huismans, Y., and Kästner, K. (2017). Tidal controls on river delta morphology. *Nat. Geosci.* 10 (9), 637–645. doi:10.1038/ngeo3000

Hori, K., and Saito, Y. (2022). *Classification, architecture, and evolution of large river deltas. Large Rivers: geomorphology and Management*. Second Edition, 114–145.

Hsieh, H. H., Chuang, M. H., Shih, Y. Y., Weerakkody, W. S., Huang, W. J., Hung, C. C., et al. (2021). Eutrophication and hypoxia in tropical Negombo lagoon, Sri Lanka. *Front. Mar. Sci.* 8, 678832. doi:10.3389/fmars.2021.678832

Huber, B. T., MacLeod, K. G., Watkins, D. K., and Coffin, M. F. (2018). The rise and fall of the Cretaceous Hot Greenhouse climate. *Glob. Planet. Change* 167, 1–23. doi:10.1016/j.gloplacha.2018.04.004

Jank, M., Wetzel, A., and Meyer, C. A. (2006). Late jurassic sea-level fluctuations in NW Switzerland (late oxfordian to late kimmeridgian): closing the gap between the boreal and tethyan realm in western Europe. *Facies* 52 (4), 487–519. doi:10.1007/s10347-005-0044-y

Jehu, T. J. (1909). II.—the glacial deposits of western carnarvonshire. *Earth Environ. Sci. Trans. R. Soc. Edinb.* 47 (1), 17–56. doi:10.1017/s0080456800011868

Kabanov, P., Hauck, T. E., Gouwy, S. A., Grasby, S. E., and van der Boon, A. (2023). Oceanic anoxic events, photic-zone euxinia, and controversy of sea-level fluctuations during the Middle-Late Devonian. *Earth-Science Rev.* 241, 104415. doi:10.1016/j.earscirev.2023.104415

Kaminskas, D., Michelevičius, D., and Blažauskas, N. (2015). New evidence of an early Pridoli barrier reef in the southern part of the Baltic Silurian basin based on three-dimensional seismic survey, Lithuania. *Est. J. earth Sci.* 64 (1), 47–55. doi:10.3176/earth.2015.09

Kaufman, D. S., and Broadman, E. (2023). Revisiting the Holocene global temperature conundrum. *Nature* 614 (7948), 425–435. doi:10.1038/s41586-022-05536-w

Kell-Duivestein, I. J., Baldermann, A., Mavromatis, V., and Dietzel, M. (2019). Controls of temperature, alkalinity and calcium carbonate reactant on the evolution of dolomite and magnesite stoichiometry and dolomite cation ordering degree-An experimental approach. *Chem. Geol.* 529, 119292. doi:10.1016/j.chemgeo.2019.119292

Kershaw, S., Crasquin, S., Forel, M. B., Randon, C., Collin, P., Kosun, E., et al. (2011). Earliest Triassic microbialites in Çürük Dag, southern Turkey: composition, sequences and controls on formation. *Sedimentology* 58 (3), 739–755. doi:10.1111/j.1365-3091.2010.01181.x

Knoll, A. H., Javaux, E. J., Hewitt, D., and Cohen, P. (2006). Eukaryotic organisms in Proterozoic oceans. *Philosophical Trans. R. Soc. B Biol. Sci.* 361 (1470), 1023–1038. doi:10.1098/rstb.2006.1843

Kontakiotis, G., Butiseacă, G. A., Antonarakou, A., Agiadi, K., Zarkogiannis, S. D., Krsnik, E., et al. (2022). Hypersalinity accompanies tectonic restriction in the eastern Mediterranean prior to the Messinian Salinity Crisis. *Palaeogeogr. Palaeoclimatol. Palaeoecol.* 592, 110903. doi:10.1016/j.palaeo.2022.110903

Krijgsman, W., Rohling, E. J., Palcu, D. V., Raad, F., Amarathunga, U., Flecker, R., et al. (2024). Causes and consequences of the Messinian salinity crisis. *Nat. Rev. Earth and Environ.*, 1–16. doi:10.1038/s43017-024-00533-1

Lan, Z., Zhang, S., Tucker, M., Li, Z., and Zhao, Z. (2020). Evidence for microbes in early Neoproterozoic stromatolites. *Sediment. Geol.* 398, 105589. doi:10.1016/j.sedgeo.2020.105589

Large, R. R., Hazen, R. M., Morrison, S. M., Gregory, D. D., Steadman, J. A., and Mukherjee, I. (2022). Evidence that the GOE was a prolonged event with a peak around 1900 Ma. *Geosystems Geoenvironment* 1 (2), 100036. doi:10.1016/j.geogeo.2022.100036

Le Hir, P., Monbet, Y., and Orvain, F. (2007). Sediment erodability in sediment transport modelling: can we account for biota effects? *Cont. Shelf Res.* 27 (8), 1116–1142. doi:10.1016/j.csr.2005.11.016

Leroux, E., Aslanian, D., Rabineau, M., Pellen, R., and Moulin, M. (2018). The late Messinian event: a worldwide tectonic revolution. *Terra nova.* 30 (3), 207–214. doi:10.1111/ter.12327

Li, J., Dada, A., Puladi, B., Kleesiek, J., and Egger, J. (2024). ChatGPT in healthcare: a taxonomy and systematic review. *Comput. Methods Programs Biomed.* 245, 108013. doi:10.1016/j.cmpb.2024.108013

Liu, S., Bao, H., Sun, G., Wang, W., Fu, J., Gao, L., et al. (2022). Archean crust-mantle geodynamic regimes: a review. *Geosystems Geoenvironment* 1 (3), 100063. doi:10.1016/j.geogeo.2022.100063

Louis-Schmid, B., Rais, P., Schaeffer, P., Bernasconi, S. M., and Weissert, H. (2007). Plate tectonic trigger of changes in pCO2 and climate in the Oxfordian (Late Jurassic): carbon isotope and modeling evidence. *Earth Planet. Sci. Lett.* 258 (1-2), 44–60. doi:10.1016/j.epsl.2007.03.014

Lowe, D. R. (1994). Abiological origin of described stromatolites older than 3.2 Ga. *Geology* 22 (5), 387–390. doi:10.1130/0091-7613(1994)022<0387:aoodso>2.3.co;2

Lü, C., Wu, S., Yao, Y., and Fulthorpe, C. S. (2013). Development and controlling factors of Miocene carbonate platform in the nam con son basin, southwestern South China sea. *Mar. Petroleum Geol.* 45, 55–68. doi:10.1016/j.marpetgeo.2013.04.014

Lyons, T. W., Reinhard, C. T., and Planavsky, N. J. (2014). The rise of oxygen in Earth's early ocean and atmosphere. *Nature* 506 (7488), 307–315. doi:10.1038/nature13068

Marcilly, C. M., Maffre, P., Le Hir, G., Pohl, A., Fluteau, F., Goddéris, Y., et al. (2022). Understanding the early Paleozoic carbon cycle balance and climate change from modelling. *Earth Planet. Sci. Lett.* 594, 117717. doi:10.1016/j.epsl.2022.117717

Martin-Bello, L., Arenas, C., Andrews, J. E., Alonso-Zarza, A. M., and Marca, A. (2019). Lacustrine stromatolites as multi-scale recorders of climate change: insights from the Miocene Ebro Basin. *Palaeogeogr. Palaeoclimatol. Palaeoecol.* 530, 312–329. doi:10.1016/j.palaeo.2019.05.001

Mary, M., and Woods, A. D. (2008). Stromatolites of the lower triassic union wash formation, CA: evidence for continued post-extinction environmental stress in western North America through the spathian. *Palaeogeogr. Palaeoclimatol. Palaeoecol.* 261 (1-2), 78–86. doi:10.1016/j.palaeo.2008.01.008

McCall, J. (2010). Lake Bogoria, Kenya: hot and warm springs, geysers and Holocene stromatolites. *Earth-Science Rev.* 103 (1-2), 71–79. doi:10.1016/j.earscirev.2010.08.001

Morse, J. (2003). *Formation and diagenesis of carbonate sediments[M]//holland H D, turekian K K. Treatise on geochemistry*. Pergamon Press, 67–85.

Müller, R. D., Flament, N., Cannon, J., Tetley, M. G., Williams, S. E., Cao, X., et al. (2022). A tectonic-rules-based mantle reference frame since 1 billion years ago–implications for supercontinent cycles and plate–mantle system evolution. *Solid earth.* 13 (7), 1127–1159. doi:10.5194/se-13-1127-2022

Nardin, E., Goddéris, Y., Donnadieu, Y., Hir, G. L., Blakey, R. C., Pucéat, E., et al. (2011). Modeling the early Paleozoic long-term climatic trend. *Bulletin* 123 (5-6), 1181–1192. doi:10.1130/b30364.1

Nutman, A. P., Bennett, V. C., Friend, C. R. L., Van Kranendonk, M. J., and Chivas, A. R. (2016). Rapid emergence of life shown by discovery of 3,700-million-year-old microbial structures. *Nature* 537 (7621), 535–538. doi:10.1038/nature19355

Obrador, B., and Pretus, J. L. (2008). Light regime and components of turbidity in a Mediterranean coastal lagoon. *Estuar. Coast. Shelf Sci.* 77 (1), 123–133. doi:10.1016/j.ecss.2007.09.008

Och, L. M., and Shields-Zhou, G. A. (2012). The Neoproterozoic oxygenation event: environmental perturbations and biogeochemical cycling. *Earth-Science Rev.* 110 (1-4), 26–57. doi:10.1016/j.earscirev.2011.09.004

Olivier, N., Pittet, B., and Mattioli, E. (2004). Palaeoenvironmental control on sponge-microbialite reefs and contemporaneous deep-shelf marl-limestone deposition (Late Oxfordian, southern Germany). *Palaeogeogr. Palaeoclimatol. Palaeoecol.* 212 (3-4), 233–263. doi:10.1016/s0031-0182(04)00313-x

Osco, L. P., Lemos, E. L., Gonçalves, W. N., Ramos, A. P. M., and Marcato Junior, J. (2023). The potential of visual ChatGPT for remote sensing. *Remote Sens.* 15 (13), 3232. doi:10.3390/rs15133232

Ovalle, A. R. C., Rezende, C. E., Lacerda, L. D., and Silva, C. (1990). Factors affecting the hydrochemistry of a mangrove tidal creek, Sepetiba Bay, Brazil. *Estuar. Coast. Shelf Sci.* 31 (5), 639–650. doi:10.1016/0272-7714(90)90017-l

Perovich, D. K., Richter-Menge, J. A., Jones, K. F., and Light, B. (2008). Sunlight, water, and ice: extreme Arctic sea ice melt during the summer of 2007. *Geophys. Res. Lett.* 35 (11), L11501. doi:10.1029/2008gl034007

Peters, S. E., Husson, J. M., and Wilcots, J. (2017). The rise and fall of stromatolites in shallow marine environments. *Geology* 45 (6), 487–490. doi:10.1130/g38931.1

Peters, S. E., and McClennen, M. (2016). The Paleobiology Database application programming interface. *Paleobiology* 42 (1), 1–7. doi:10.1017/pab.2015.39

Petrash, D. A., Robbins, L. J., Shapiro, R. S., Mojzsis, S., and Konhauser, K. (2016). Chemical and textural overprinting of ancient stromatolites: timing, processes, and implications for their use as paleoenvironmental proxies. *Precambrian Res.* 278, 145–160. doi:10.1016/j.precamres.2016.03.010

Petryshyn, V. A., Rivera, M. J., Agić, H., Frantz, C. M., Corsetti, F. A., and Tripati, A. E. (2016). Stromatolites in Walker Lake (Nevada, Great Basin, USA) record climate

and lake level changes~ 35,000 years ago. *Palaeogeogr. Palaeoclimatol. Palaeoecol.* 451, 140–151. doi:10.1016/j.palaeo.2016.02.054

Pfefferkorn, H. W., Alleman, V., and Iannuzzi, R. (2014). A greenhouse interval between icehouse times: climate change, long-distance plant dispersal, and plate motion in the Mississippian (late Visean–earliest Serpukhovian) of Gondwana. *Gondwana Res.* 25 (4), 1338–1347. doi:10.1016/j.gr.2013.08.022

Piotrowska, N., Pazdur, A., Pawełczyk, S., Rakowski, A. Z., Sensuła, B., and Tudyka, K. (2020). Human activity recorded in carbon isotopic composition of atmospheric CO2 in Gliwice urban area and surroundings (southern Poland) in the years 2011–2013. *Radiocarbon* 62 (1), 141–156. doi:10.1017/rdc.2019.92

Planavsky, N. J., Tarhan, L. G., Bellefroid, E. J., Evans, D. A., Reinhard, C. D., Love, G. D., et al. (2015). Late Proterozoic transitions in climate, oxygen, and tectonics, and the rise of complex life[M]//Polly D, Head J J, Fox D L. Earth-life transitions: paleobiology in the context of earth system evolution, the Paleontological Society Short Course. *Paleontological Soc.* 21, 1–36. doi:10.1017/s1089332600002965

Pohl, A., Donnadieu, Y., Godderis, Y., Lanteaume, C., Hairabian, A., Frau, C., et al. (2020). Carbonate platform production during the Cretaceous. *GSA Bull.* 132 (11-12), 2606–2610. doi:10.1130/b35680.1

Polverini, G., and Gregorcic, B. (2024). How understanding large language models can inform the use of ChatGPT in physics education. *Eur. J. Phys.* 45 (2), 025701. doi:10.1088/1361-6404/ad1420

Porter, S. M., and Riedman, L. A. (2023). Frameworks for interpreting the early fossil record of eukaryotes. *Annu. Rev. Microbiol.* 77 (1), 173–191. doi:10.1146/annurev-micro-032421-113254

Price, G. D., and Rogov, M. A. (2009). An isotopic appraisal of the Late Jurassic greenhouse phase in the Russian Platform. *Palaeogeogr. Palaeoclimatol. Palaeoecol.* 273 (1-2), 41–49. doi:10.1016/j.palaeo.2008.11.011

Rakib, M. R. J., Hossain, M. B., Islam, M. S., Hossain, I., Rahman, M. M., Kumar, R., et al. (2022). Ecohydrological features and biodiversity status of estuaries in Bengal delta, Bangladesh: a comprehensive review. *Front. Environ. Sci.* 10, 990099. doi:10.3389/fenvs.2022.990099

Rao, V. P., Rao, K. M., and Raju, D. S. N. (2000). Quaternary phosphorites from the continental margin off Chennai, southeast India: analogs of ancient phosphate stromatolites. *J. Sediment. Res.* 70 (5), 1197–1209. doi:10.1306/012400701197

Rautio, M., Bayly, I. A., Gibson, J. A., and Nyman, M. (2008). *Zooplankton and zoobenthos in high-latitude water bodies[M]//vincent W, laybourn-parry J. Polar lakes and rivers: limnology of arctic and antarctic aquatic ecosystems*. New York: Oxford University Press, 231–247.

Ray, D. C., van Buchem, F. S. P., Baines, G., Davies, A., Gréselle, B., Simmons, M. D., et al. (2019). The magnitude and cause of short-term eustatic Cretaceous sea-level change: a synthesis. *Earth-Science Rev.* 197, 102901. doi:10.1016/j.earscirev.2019.102901

Ray, P. P. (2024). ChatGPT in transforming communication in seismic engineering: case studies, implications, key challenges and future directions. *Earthq. Sci.* 37 (4), 352–367. doi:10.1016/j.eqs.2024.04.003

Riaz, M., Xiao, E., Latif, K., and Zafar, T. (2019). Sequence-stratigraphic position of oolitic bank of cambrian in North China platform: example from the kelan section of shanxi province. *Arabian J. Sci. Eng.* 44, 391–407. doi:10.1007/s13369-018-3403-z

Ridderinkhof, H. (2019). *Sediment transport in intertidal areas[M]//Eisma D. Intertidal deposits: river mouths, tidal flats, and coastal lagoons*. Florida: CRC Press, 363–382.

Riding, R. (2000). Microbial carbonates: the geological record of calcified bacterial–algal mats and biofilms. *Sedimentology* 47, 179–214. doi:10.1046/j.1365-3091.2000.00003.x

Riding, R. (2005). Phanerozoic reefal microbial carbonate abundance: comparisons with metazoan diversity, mass extinction events, and seawater saturation state. *Rev. Española Micropaleontol.* 37 (1), 23–39.

Riding, R. (2006). Microbial carbonate abundance compared with fluctuations in metazoan diversity over geological time. *Sediment. Geol.* 185 (3-4), 229–238. doi:10.1016/j.sedgeo.2005.12.015

Sames, B., Wagreich, M., Wendler, J. E., Haq, B., Conrad, C., Melinte-Dobrinescu, M., et al. (2016). Review: short-term sea-level changes in a greenhouse world — a view from the Cretaceous. *Palaeogeogr. Palaeoclimatol. Palaeoecol.* 441, 393–411. doi:10.1016/j.palaeo.2015.10.045

Schirrmeister, B. E., de Vos, J. M., Antonelli, A., and Bagheri, H. C. (2013). Evolution of multicellularity coincided with increased diversification of cyanobacteria and the Great Oxidation Event. *Proc. Natl. Acad. Sci.* 110 (5), 1791–1796. doi:10.1073/pnas.1209927110

Schirrmeister, B. E., Sanchez-Baracaldo, P., and Wacey, D. (2016). Cyanobacterial evolution during the precambrian. *Int. J. Astrobiol.* 15 (3), 187–204. doi:10.1017/s1473550415000579

Schubert, H., and Telesh, I. (2017). "Estuaries and coastal lagoons." in *Biological oceanography of the baltic sea*, 483–509.

Schubert, J. K., and Bottjer, D. J. (1992). Early Triassic stromatolites as post-mass extinction disaster forms. *Geology* 20 (10), 883–886. doi:10.1130/0091-7613(1992)020<0883:etsapm>2.3.co;2

Scotese, C. R., Vérard, C., Burgener, L., Elling, R. p., and Kocsis, A. P. (2025). The cretaceous world: plate tectonics, paleogeography, and paleoclimate. *Geol. Soc. Lond. Spec. Publ.* 544 (1), SP544-2024–2028. doi:10.1144/sp544-2024-28

Sebastiá-Frasquet, M. T., Aguilar-Maldonado, J. A., Santamaría-Del-Ángel, E., and Estornell, J. (2019). Sentinel 2 analysis of turbidity patterns in a coastal lagoon. *Remote Sens.* 11 (24), 2926. doi:10.3390/rs11242926

Sergeev, V. N., Sharma, M., and Shukla, Y. (2012). Proterozoic fossil cyanobacteria. *Palaeobot.* 61, 189–358. doi:10.54991/jop.2012.359

Shao, L., Cui, Y., Qiao, P., Zhang, D., Liu, X., and Zhang, C. (2017). Sea-Level changes and carbonate platform evolution of the xisha islands (South China Sea) since the early Miocene. *Palaeogeogr. Palaeoclimatol. Palaeoecol.* 485, 504–516. doi:10.1016/j.palaeo.2017.07.006

Shtienberg, G., Cantu, K., Mischke, S., Sivan, D., Norris, R. D., Rittenour, T. M., et al. (2022). Holocene sea-level rise and coastal aquifer interactions: triggering mechanisms for environmental change and impacts on human settlement patterns at Dor, Israel. *Quat. Sci. Rev.* 294, 107740. doi:10.1016/j.quascirev.2022.107740

Silveira, L. F., Borghi, L., Bobco, F. E. R., Araújo, B. C., Kroth, M., Duarte, G., et al. (2023). Multiscale characterization of an extensive stromatolite field: a new correlation horizon for the Crato Member, Araripe Basin, Brazil. *J. Sediment. Res.* 93 (10), 776–795. doi:10.2110/jsr.2022.090

Simms, M. J., and Ruffell, A. H. (2018). The Carnian Pluvial Episode: from discovery, through obscurity, to acceptance. *J. Geol. Soc.* 175 (6), 989–992. doi:10.1144/jgs2018-020

Simon, D., and Meijer, P. T. (2017). Salinity stratification of the Mediterranean Sea during the Messinian crisis: a first model analysis. *Earth Planet. Sci. Lett.* 479, 366–376. doi:10.1016/j.epsl.2017.09.045

Somerville, I. D., Cózar, P., Aretz, M., Herbig, H. G., Mitchell, W. I., and Medina-Varea, P. (2009). Carbonate facies and biostromal distribution in a tectonically controlled platform in northwest Ireland during the late Viséan (Mississippian). *Proc. Yorks. Geol. Soc.* 57 (3-4), 165–192. doi:10.1144/pygs.57.3-4.165

Steinthorsdottir, M., Coxall, H. K., De Boer, A. M., Huber, M., Barbolini, N., Bradshaw, C. D., et al. (2021). The Miocene: the future of the past. *Paleoceanogr. Paleoclimatology* 36 (4), e2020PA004037. doi:10.1029/2020pa004037

Stibal, M., Šabacká, M., and Žárský, J. (2012). Biological processes on glacier and ice sheet surfaces. *Nat. Geosci.* 5 (11), 771–774. doi:10.1038/ngeo1611

Stüeken, E. E., and Buick, R. (2018). Environmental control on microbial diversification and methane production in the Mesoarchean. *Precambrian Res.* 304, 64–72. doi:10.1016/j.precamres.2017.11.003

Teichert, S. (2014). Hollow rhodoliths increase Svalbard's shelf biodiversity. *Sci. Rep.* 4 (1), 6972. doi:10.1038/srep06972

Tierney, J. E., Haywood, A. M., Feng, R., Bhattacharya, T., and Otto-Bliesner, B. L. (2019). Pliocene warmth consistent with greenhouse gas forcing. *Geophys. Res. Lett.* 46 (15), 9136–9144. doi:10.1029/2019gl083802

Toneatti, D. M., Albarracín, V. H., Flores, M. R., Polerecky, L., and Farías, M. E. (2017). Stratified bacterial diversity along physico-chemical gradients in high-altitude modern stromatolites. *Front. Microbiol.* 8, 646. doi:10.3389/fmicb.2017.00646

Trower, E. J., Cantine, M. D., Gomes, M. L., Grotzinger, J. P., Knoll, A. H., Lamb, M. P., et al. (2018). Active ooid growth driven by sediment transport in a high-energy shoal, Little Ambergris Cay, Turks and Caicos Islands. *J. Sediment. Res.* 88 (9), 1132–1151. doi:10.2110/jsr.2018.59

Vacek, F., Slavík, L., Sobień, K., and áp, P. (2018). Refining the late Silurian sea-level history of the Prague Syncline—a case study based on the Přídolí GSSP (Czech Republic). *Facies* 64, 1–16. doi:10.1007/s10347-018-0542-3

Vandenbroucke, T. R. A., Emsbo, P., Munnecke, A., Nuns, N., Duponchel, L., Lepot, K., et al. (2015). Metal-induced malformations in early Palaeozoic plankton are harbingers of mass extinction. *Nat. Commun.* 6 (1), 7966. doi:10.1038/ncomms8966

Vasconcelos, A. G., Bittencourt, J. S., Eliziário, N. F., Kraemer, B. M., Auler, A. S., et al. (2020). Stromatolites in caves in southeastern Brazil and their importance to geoconservation. *Geoheritage* 12, 1–19. doi:10.1007/s12371-020-00469-0

Vasiliev, I., Mezger, E. M., Lugli, S., Reichart, G. J., Manzi, V., and Roveri, M. (2017). How dry was the Mediterranean during the Messinian salinity crisis. *Palaeogeogr. Palaeoclimatol. Palaeoecol.* 471, 120–133. doi:10.1016/j.palaeo.2017.01.032

Vieira, F. V., Bastos, A. C., Quaresma, V. S., Leite, M. D., Costa, A., Jr., Oliveira, K. S., et al. (2019). Along-shelf changes in mixed carbonate-siliciclastic sedimentation patterns. *Cont. Shelf Res.* 187, 103964. doi:10.1016/j.csr.2019.103964

Wang, J. P., Li, Q. J., Kershaw, S., Zhang, Y. Y., Yu, S. Y., and Li, Y. (2021). Late tremadocian (early ordovician) reefs on the yangtze platform, South China, and their geobiological implications: a synthesis. *J. Palaeogeogr.* 10, 6–15. doi:10.1186/s42501-021-00086-0

Wang, T., Burne, R. V., Yuan, A., Wang, Y., and Yi, Z. (2019). The evolution of microbialite forms during the Early Triassic transgression: a case study in Chongyang of Hubei Province, South China. *Palaeogeogr. Palaeoclimatol. Palaeoecol.* 519, 209–220. doi:10.1016/j.palaeo.2018.01.043

Warke, M. R., Di Rocco, T., Zerkle, A. L., Lepland, A., Prave, A. R., Martin, A. P., et al. (2020). The great oxidation event preceded a paleoproterozoic "snowball Earth". *Proc. Natl. Acad. Sci.* 117 (24), 13314–13320. doi:10.1073/pnas.2003090117

Wei, S. H., and Tian, J. (2022). Mechanisms of greenhouse climate at low atmospheric CO 2 levels in the Late Miocene. *Adv. Earth Sci.* 37 (4), 417. doi:10.11867/j.issn.1001-8166.2021.116

Wheatcroft, R. A., and Sommerfield, C. K. (2005). River sediment flux and shelf sediment accumulation rates on the Pacific Northwest margin. *Cont. shelf Res.* 25 (3), 311–332. doi:10.1016/j.csr.2004.10.001

Willeit, M., Ganopolski, A., Calov, R., and Brovkin, V. (2019). Mid-Pleistocene transition in glacial cycles explained by declining CO2 and regolith removal. *Sci. Adv.* 5 (4), eaav7337. doi:10.1126/sciadv.aav7337

Winter, C., Katoshevski, D., Bartholomä, A., and Flemming, B. W. (2007). Grouping dynamics of suspended matter in tidal channels. *J. Geophys. Res. Oceans* 112, C08010. doi:10.1029/2005jc003423

Wood, P. J., and Armitage, P. D. (1997). Biological effects of fine sediment in the lotic environment. *Environ. Manag.* 21 (2), 203–217. doi:10.1007/s002679900019

Wright, L. D. (1977). Sediment transport and deposition at river mouths: a synthesis. *Geol. Soc. Am. Bull.* 88 (6), 857–868. doi:10.1130/0016-7606(1977)88<857:stadar>2.0.co;2

Xiong, H., Zong, Y., Qian, P., Huang, G., and Fu, S. (2018). Holocene sea-level history of the northern coast of South China Sea. *Quat. Sci. Rev.* 194, 12–26. doi:10.1016/j.quascirev.2018.06.022

Yamamoto, M., Clemens, S. C., Seki, O., Tsuchiya, Y., Huang, Y., O'ishi, R., et al. (2022). Increased interglacial atmospheric CO2 levels followed the mid-Pleistocene Transition. *Nat. Geosci.* 15 (4), 307–313. doi:10.1038/s41561-022-00918-1

Yao, L., Wang, X., Lin, W., Li, Y., Kershaw, S., and Qie, W. (2016). Middle Viséan (Mississippian) coral biostrome in central Guizhou, southwestern China and its palaeoclimatological implications. *Palaeogeogr. Palaeoclimatol. Palaeoecol.* 448, 179–194. doi:10.1016/j.palaeo.2015.08.031

Yoo, J. W., Lee, Y. W., Lee, C. G., and Kim, C. S. (2013). Effective prediction of biodiversity in tidal flat habitats using an artificial neural network. *Mar. Environ. Res.* 83, 1–9. doi:10.1016/j.marenvres.2012.10.001

Yue, X. L., and Gao, Q. X. (2018). Contributions of natural systems and human activity to greenhouse gas emissions. *Adv. Clim. Change Res.* 9 (4), 243–252. doi:10.1016/j.accre.2018.12.003

Zhai, M., Zhu, X., Zhou, Y., Zhao, L., and Zhou, L. (2020). Continental crustal evolution and synchronous metallogeny through time in the North China Craton. *J. Asian Earth Sci.* 194, 104169. doi:10.1016/j.jseaes.2019.104169

Zhang, F., Xu, H., Konishi, H., Shelobolina, E. S., and Roden, E. E. (2012). Polysaccharide-catalyzed nucleation and growth of disordered dolomite: a potential precursor of sedimentary dolomite. *Am. Mineralogist* 97 (4), 556–567. doi:10.2138/am.2012.3979

Zhang, J., Du, Y. N., Zhang, G. S., Chang, Y., Zhou, Y. C., Zhang, Z. F., et al. (2021). Increases in the seaward river flux of nutrients driven by human migration and land-use changes in the tide-influenced delta. *Sci. Total Environ.* 761, 144501. doi:10.1016/j.scitotenv.2020.144501

Zhang, L., Chen, D., Huang, T., Yu, H., Zhou, X., and Wang, J. (2020). An abrupt oceanic change and frequent climate fluctuations across the Frasnian–Famennian transition of Late Devonian: constraints from conodont Sr isotope. *Geol. J.* 55 (6), 4479–4492. doi:10.1002/gj.3657

Zhang, X., Fagherazzi, S., Leonardi, N., and Li, J. (2018). A positive feedback between sediment deposition and tidal prism may affect the morphodynamic evolution of tidal deltas. *J. Geophys. Res. Earth Surf.* 123 (11), 2767–2783. doi:10.1029/2018jf004639

Zhang, X., Li, H., Liu, Q., Li, Z., Reymond, C. E., Zhang, M., et al. (2023). A new machine-learning extracting approach to construct a knowledge base: a case study on global stromatolites over geological time. *J. Earth Sci.* 34 (5), 1358–1373. doi:10.1007/s12583-022-1801-3

Zhang, Y., Li, Q., Li, Y., Kiessling, W., and Wang, J. (2016). Cambrian to lower ordovician reefs on the yangtze platform, South China block, and their controlling factors. *Facies* 62, 17–18. doi:10.1007/s10347-016-0466-8

Zhou, Q., Chen, W., Shan, K., Zheng, L., and Song, L. (2014). Influence of sunlight on the proliferation of cyanobacterial blooms and its potential applications in Lake Taihu, China. *J. Environ. Sci.* 26 (3), 626–635. doi:10.1016/s1001-0742(13)60457-x